AD-A151 107 AN INVESTIGATION OF THE STRUCTURE AND HIGH TEMPERATURE MECHANICAL PROPERT..(U) STANFORD UNIV CA DEPT OF MATERIALS SCIENCE AND ENGINEERING W D NIX DEC 84 1/1

UNCLASSIFIED AFOSR-TR-85-0164 AFOSR-81-0022 F/G 11/6 NL

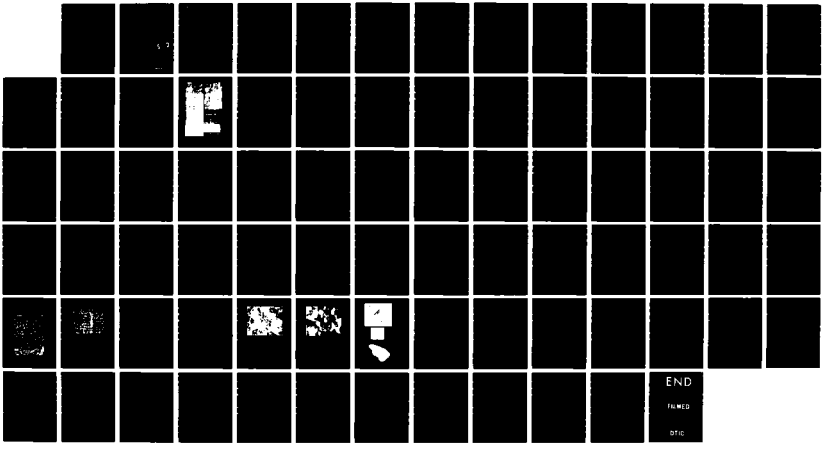

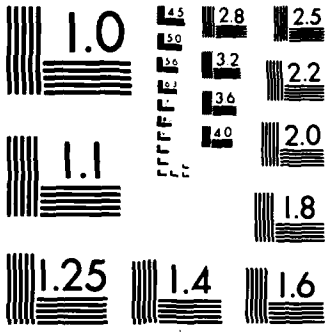

UNCLASSIFIED

(3)

SECURITY CLASSIFICATION OF THIS PAGE (When Data Entered)

Caplan

REPORT DOCUMENTATION PAGE		READ INSTRUCTIONS BEFORE COMPLETING FORM
1. REPORT NUMBER AFOSR-TR- 85-0164	2. GOVT ACCESSION NO.	3. RECIPIENT'S CATALOG NUMBER
4. TITLE (and Subtitle) An Investigation of the Structure and High Temperature Mechanical Properties of Oxide Dispersion Strengthened Alloys		5. TYPE OF REPORT & PERIOD COVERED Interim Scientific Report 1 Oct 83 - 30 Sep 84
		6. PERFORMING ORG. REPORT NUMBER
7. AUTHOR(s) William D. Nix, Professor		8. CONTRACT OR GRANT NUMBER(s) AFOSR 81-0022
9. PERFORMING ORGANIZATION NAME AND ADDRESS Department of Materials Science & Engineering Stanford University, Stanford, California 94305		10. PROGRAM ELEMENT, PROJECT, TASK AREA & WORK UNIT NUMBERS 61102F 2306, A1
11. CONTROLLING OFFICE NAME AND ADDRESS Air Force Office of Scientific Research (NE) Bolling AFB, Bldg. 410, Washington, D.C. 20332		12. REPORT DATE December 1984
		13. NUMBER OF PAGES 76
14. MONITORING AGENCY NAME & ADDRESS (if different from Controlling Office) ATTENTION: DR, IVAN CAPLAN		15. SECURITY CLASS. (of this report) Unclassified
		15a. DECLASSIFICATION/DOWNGRADING SCHEDULE

16. DISTRIBUTION STATEMENT (of this Report)

Approved for public release; distribution unlimited.

17. DISTRIBUTION STATEMENT (of the abstract entered in Block 20, if different from Report)

DTIC ELECTE MAR 13 1985 S D E

18. SUPPLEMENTARY NOTES

19. KEY WORDS (Continue on reverse side if necessary and identify by block number)

Oxide dispersion strengthened metals, solute strengthening, dispersion strengthening, ODS superalloys, superplasticity, creep strength.

20. ABSTRACT (Continue on reverse side if necessary and identify by block number)

The structure and high temperature mechanical properties of oxide dispersion strengthened alloys are being studied. We have studied the creep and fracture properties of Inconel MA754 at very high temperatures. These properties depend both on the size distributions of the Y_2O_3 dispersoids (which have been measured with small angle X-ray scattering) and on the morphology of the grain structure. We have also studied the high temperature flow properties of Al-Fe-Ce alloys made by RSR techniques. We have shown that the particles which strengthen this alloy are monoclinic $Al_{13}Fe_4$. The high temperature strength of the alloy is →

DD FORM 1 JAN 73 1473 EDITION OF 1 NOV 65 IS OBSOLETE S/N 0102-LF-014-6601

42. SECURITY CLASSIFICATION OF THIS PAGE (When Data Entered) UNCLASSIFIED

AD-A151 107

DTIC FILE COPY

85 02 28 004

found to be limited both by coarsening of the precipitates and by precipitate twinning. Efforts to improve the high temperature strength of Al-Fe-Ce by mechanical alloying are underway. These studies include the development of techniques for making TEM thin foils from powders.

Abstract - supplied keywords included. T, col p.

INTERIM SCIENTIFIC REPORT

(For the Period 1 October 1983 to 30 September 1984)

(AFOSR GRANT NO. 81 - 0022C)

AN INVESTIGATION OF THE STRUCTURE AND HIGH TEMPERATURE MECHANICAL PROPERTIES OF OXIDE DISPERSION STRENGTHENED ALLOYS

Submitted to

Department of the Air Force

Directorate of Electronic and Solid State Sciences

Air Force Office of Scientific Research

Bolling AFB, Building 410, Washington, D.C. 20332

ATTN: Dr. Ivan Caplan

Submitted by

Professor William D. Nix (Principal Investigator)

Department of Materials Science and Engineering

Stanford University, Stanford, California 94305

December 1984

This research was supported by the Air Force Office of Scientific Research (AFOSR) under Grant No. AFOSR 81 - 0022

TABLE OF CONTENTS

I. SUMMARY OF RESEARCH

The overall objective of this research has been to develop a better understanding of the structure and high temperature mechanical properties of oxide dispersion strengthened metals. In this report we describe some of the progress we have made during the past year.

Our work on the high temperature creep and fracture properties of Inconel MA 754 is nearing completion. We have completed extensive characterization studies of this material as well as studies of the creep and fracture properties at very high temperatures. As reported last year, two major creep regimes have been discovered. At relatively high stresses, creep flow appears to be limited by interactions between dislocations and dispersoids. The creep properties are very similar to those found for ODS single crystals. Deformation is relatively homogenous and fracture is transgranular. High stress exponents associated with dislocation pinning are observed. In this regime the creep strength depends sensitively on the mean spacing between dispersoids. As reported here, we have studied the dispersoid distributions in two heats of MA 754 using small angle X-ray scattering techniques. In this way we have measured the mean spacing between dispersoids in the two heats. We find the creep strength correlates almost perfectly with the dispersoid spacing. The heat with the higher dispersoid content exhibits 25% higher creep strengths. This compares well with the 25% smaller spacing between dispersoids.

At low stresses creep is inhomogeneous and fracture is intergranular. Here the heat with the highest dispersoid content is much weaker than the heat containing fewer dispersoids. This unusual result can be explained by

considering that creep occurs by intergranular cavitation in this regime. Models for creep by cavitation have been developed to account for the behavior of the two heats. The heat with the higher dispersoid content also has a duplex grain structure with very fine grains being present on many of the longitudinal grain boundaries. These fine grains permit the longitudinal boundaries to slide and this in turn permits cavitation to occur on the transverse grain boundaries at a rapid rate. In this way the heat with the highest dispersoid content is weakest at low stresses.

Our studies of MA 754 have clearly shown the balance which must be struck when creating ODS alloys for use at high temperatures. The dispersoid content must be as high as possible to obtain the highest possible resistance to dislocation motion, but a uniformly coarse grain structural must also be achieved. In practice it may be necessary to limit the dispersoid content so that a uniform coarse grain structure can be achieved.

Our work on Al-Fe-Ce alloys has included high temperature deformation studies and mechanical alloying of Al - 8.4% Fe - 3.6% Ce made by RSR techniques.Our deformation studies have focused on the reasons for the loss of strength at elevated temperature. Unlike ODS aluminum, the RSR alloys become quite weak at high temperatures. Although some coarsening of the microstructure occurs at elevated temperatures, this is not sufficient to account for the loss of strength. Recent TEM studies have shown that the hardening phase present in this alloy is Al_{13} Fe_4. We have shown that this phase twins extensively at high temperatures. This suggests that the loss of strength at high temperatures in this alloy is caused by deformation of the precipitate phase. Although the Al_{13} Fe_4 precipitates appear to represent strong obstacles to dislocation motion at low temperatures, they deform by twinning at high

temperatures. This appears to represent a fundamental limitation in the ability of Al-Fe-Ce alloys to resist deformation at high temperatures. Our results suggest that even if no coarsening of the microstructure occurred at high temperatures, the alloy would still lose its strength as the precipitate particles deform by twinning.

One possible solution to the softening problem described above involves the creation of non-deformable phases in the microstructure. Mechanical alloying is being used to alter the structure of powders of Al-Fe-Ce. It is expected that Al_2O_3 and Al_4C_3 will be formed in mechanically alloyed powders and that these phases will remain undeformable at high temperatures. Our work on mechanical alloying during the past year involves primarily the characterization of the mechanical alloying process in Al-Fe-Ce powders. This research has permitted us to establish the optimum conditions for mechanical alloying and to determine some of the procedures that will be followed during subsequent consolidation and processing.

A full understanding of the mechanical alloying process will not be achieved until we are able to use TEM techniques to follow the structure evolution during processing. During the past year a considerable effort has been made to devise new techniques for making thin foil TEM samples from powders. As yet we do not have a reliable method developed but the progress we have made is sufficient to sustain our hope that TEM techniques can be used to study powder processing in the near future.

Determination of Dispersoid Size Distributions in Inconel MA 754 by Small Angle X-Ray Scattering

J.J. Stephens
Dept. of Materials Science and Engineering, Stanford University, Stanford, Ca. 94305

S. Spooner
Solid State Division, Oak Ridge National Laboratory, Oak Ridge, Tenn. 37830

The dispersoid size distribution and volume fraction of the nickel based oxide dispersion strengthened alloy Inconel MA 754 have been determined using Small Angle X-Ray Scattering (SAXS). Two methods of determining dispersoid size distributions from the SAXS spectra are utilized. One method involves a calculation of log-normal distribution parameters from the integrated intensity, forward scattering and the Porod Radius. A second method employs an integral transform of the data to calculate the size distribution. Dispersoid size distributions from the transform method exhibit close agreement with histograms obtained from thin foil Transmission Electron Microscopy. Measurement of dispersoid volume fractions from the integrated intensity, coupled with dispersoid size distributions allow a calculation of the average planar separation distance of the dispersoids. The results for two heats of MA 754 lead to predicted dislocation creep strengths which are in close agreement with creep data at 1000°C. The effect of the presence of mixed aluminum-yttrium oxides in MA 754 is considered.

Introduction

Oxide Dispersion Strengthened (ODS) nickel based alloys exhibit high creep strength at temperatures above 1000°C, and have been the focus of extensive alloy development efforts during the past two decades. The creep resistance of an ODS alloy depends directly upon the presence of finely dispersed oxide particles to inhibit dislocation motion, and indirectly upon the existence of a highly elongated grain structure to minimize grain boundary sliding (1). Development of the mechanical alloying process by Benjamin (2) and subsequent thermomechanical processing have allowed the development of commercial nickel based ODS alloys utilizing Y_2O_3 dispersoids along with sufficient reactive alloying additions such as Cr and Al to insure protective oxide scale formation. Inconel MA 754 is a commercial example of the mechanical alloying process, and has seen application as a turbine vane material in advanced jet engines (3).

The direct strengthening effect of dispersoids is usually described in terms of the Orowan bowing process. It is well known that the shear stress, τ_c, required for dislocation glide through a plane of randomly spaced point obstacles is inversely proportional to the average separation distance of the obstacles (4,5). Orowan loops are left surrounding the dispersoid as the dislocation passes the obstacle. A recent investigation of the edge dislocation-circular inclusion problem (6) evaluates the stress necessary to unpin the dislocation from the particle-matrix interface; again, the critical stress depends on the inverse of the planar dispersoid separation distance, L. Regardless of the exact model of dislocation-particle interaction examined, evaluation

of the direct strengthening effect of the oxide dispersion in an ODS alloy such as MA 754 requires the evaluation of the average planar dispersoid separation distance, $\bar{L}$. This distance can be calculated from the dispersoid size distribution and volume fraction.

Determination of the dispersoid size distribution and volume fraction in ODS alloys is, in practice, quite difficult. Bulk chemical analyses cannot give an accurate determination of volume fraction of dispersoids: the presence of Al to getter oxygen during processing in mechanically alloyed ODS alloys causes the final dispersoid volume fraction to be in excess of the nominal Y_2O_3 volume fraction. Direct methods such as thin foil transmission electron microscopy (TEM) can be utilized in order to obtain a qualitative dispersoid size distribution (7). However, the small volumes sampled (order $10^{-13}cm^3$) and wide range of diameters present (30 to $\geq$ 1000 Å) preclude determination of the true size distribution of dispersoids. The determination of dispersoid volume fraction is also quite difficult - the largest dispersoids in an electropolished TEM foil of MA 754 are a large fraction of the foil thickness (1000 to 1500 Å) and protrude from the surface of the foil. Thus, while convergent beam electron diffraction techniques (8) allow for accurate measurement of the foil thickness, protruding dispersoids lead to anomalously high dispersoid volume fractions. Similarly, extraction replicas can yield a qualitative dispersoid size distribution, but the degree of extraction varies from sample to sample and this precludes accurate determination of dispersoid volume fractions.

This paper describes the results of an investigation using the Small

Angle X-Ray Scattering (SAXS) technique for determination of the dispersoid size distribution and volume fraction in MA 754. The SAXS method allows for relatively large ($\approx 10^{-5} cm^3$) volumes to be sampled, hence large numbers of particles (10^9-10^{10}) up to diameters of 1000 Å can be included in the dispersoid size distribution. In addition, the dispersoid volume fraction can be evaluated from the integrated intensity. Average planar dispersoid separation distances can thus be calculated, and used to estimate the relative dislocation creep strength of two different heats of MA 754.

2. Experimental Procedures

Two production heats of Inconel MA 754 in the annealed (1315°C, 2 hr.) coarse grained condition were supplied by INCO. The production heat numbers are DT06A7B and DT15A5B1-1; they will be referred to as Heats 1 and 2, respectively. The chemical compositions of the two heats is shown in Table I; during the course of processing the dispersoid volume fraction increases above the nominal 1% Y_2O_3 volume fraction due to the oxidation of Al (8). Pole figure measurements (9) have revealed a strong {110}<001> rotated cube on edge texture in both heats. In order to study high temperature coarsening of the dispersoid size distribution, a 1300°C, 70 hr. anneal in 1.3×10^{-3} Pa vacuum was performed on a specimen from Heat 1. Disk specimens were spark cut from extrusion plane slices of the three conditions (Heats 1 and 2, as received (AR); Heat 1 annealed (Ann)): 7 mm diameter disks were cut for SAXS specimens, while 3 mm diameter disks were cut for TEM specimens from adjacent areas. The disks were mechanically ground to 100 μm

TABLE I. CHEMICAL COMPOSITIONS OF ALLOYS STUDIED, wt%

ALLOY	Ni	Cr	Fe	Si	Ti	Al	Y_2O_3	OXYGEN	C	S
MA 754 Heat 1	77.17	20.05	1.32	--	0.42	0.29	0.58	0.13	0.06	0.002
MA 754 Heat 2	77.66	20.53	0.19	--	0.38	0.31	0.60	0.28	0.05	-
Driver-Harris Nichrome	78.01	20.84	0.46	0.69	-	-	-	-	-	-

TABLE III. SAXS PARAMETERS

Specimen	R_g (Å)	$d\Sigma(0)/d\Omega$ (cm^{-1})	Q $(cm)^{-1}(Å)^{-3}$	R_p (Å)
Heat 1 AR	298	1.37×10^{5}	2.37×10^{-2}	140
Heat 2 AR	279	1.63×10^{5}	3.47×10^{-2}	124
Heat 1 Annealed	266	8.58×10^{4}	2.18×10^{-2}	167

of k^4 and noting the value at which a plateau in $k^4 d\Sigma(k)/d\Omega$ is reached (16). Porod's Radius, R_p, is proportional to the ratio of the integrated intensity and the Porod Constant

$$R_p = \frac{3}{\pi} \frac{Q}{p} \tag{6}$$

The values of $d\Sigma(0)/d\Omega$, Q, and R_p obtained from the scattering data are listed in Table III.

The geometric mean μ and variance σ of the log-normal distribution are obtained from the SAXS data by means of the following relations (see appendix)

$$\ln \mu = 2.25 \ln(2R_p) - \frac{1}{2.4} \ln \left(\frac{12\pi\, d\Sigma(0)/d\Omega}{Q}\right)$$
$$\ln^2 \sigma = \frac{1}{6} \ln \left(\frac{12\pi\, d\Sigma(0)/d\Omega}{Q}\right) - \frac{1}{2} \ln (2 R_p) \tag{7}$$

The log-normal parameters for the three conditions investigated are listed in Table IV. The log-normal distributions are plotted in Figs. 6, 7, and 8 for Heat 1 AR, Heat 2 AR, and Heat 1 Ann, respectively. Figure 6 shows that for Heat 1 AR there is good agreement between the SAXS log-normal distribution and the TEM data in the diameter range of 130 to 600 Å. In the case of Heat 2 AR, Fig. 7, the SAXS log-normal distribution shows agreement with the TEM data in the width of the distribution, but predicts a smaller average particle size. The same data for Heat 2 AR are plotted in histogram form in Figs. 3a and 3b. Comparison of Fig. 3b with 3a shows that the SAXS log-normal analysis is less sharply peaked than the TEM data, while the scattering

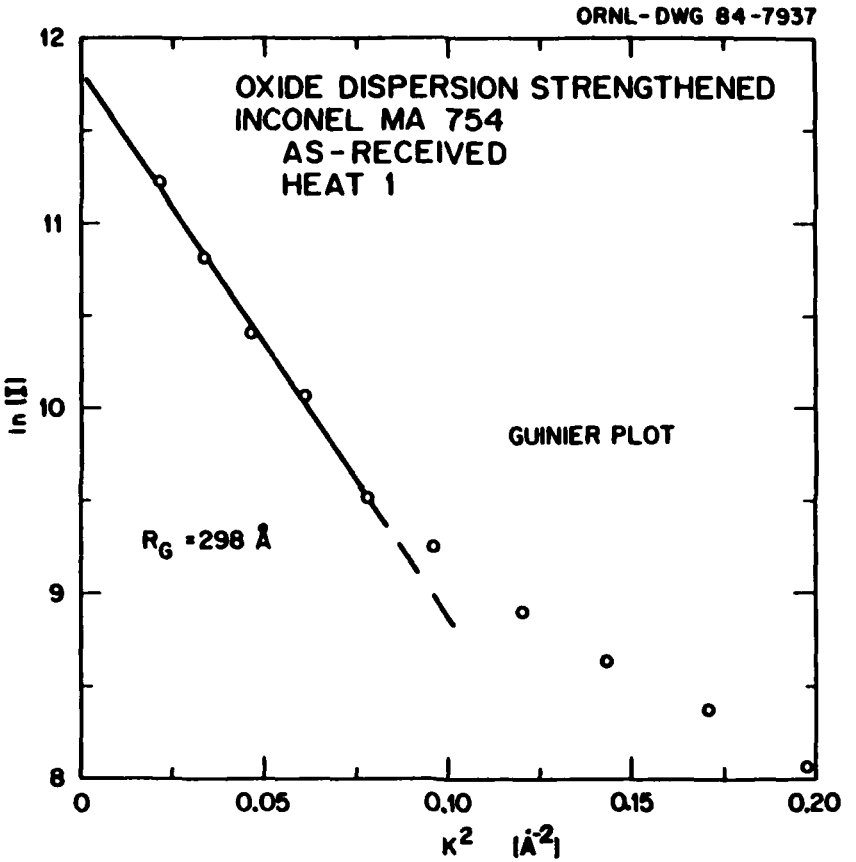

Figure 5. Guinier plot of MA 754 Heat 1 AR data. The solid line indicates the extrapolation used to obtain $d\Sigma(0)/d\Omega$ for this specimen.

TABLE II. TEM RESULTS

Sample	Histogram Data Avg. Diameter	⟨D⟩ *	Lognormal Fit μ	σ
Heat 1 AR	144 Å	142 Å	122 Å	1.73
Heat 2 AR	132 Å	126 Å	100 Å	1.97
Heat 1 Annealed	214 Å	229 Å	191 Å	1.82
As-calcined Y_2O_3	(ref. 23)	90.3 Å	71.5 Å	1.97

* Average diameter given by:
$\langle D \rangle = \exp [\ln \mu + 0.5 \ln^2 \sigma]$

II. It is evident that the dispersoid size distribution is rather broad, as indicated by the large values of σ, and that the 70 hr. annealing treatment at 1300°C increases the average diameter. The average dispersoid diameter in Heat 2 AR is found to be slightly smaller than in Heat 1 AR.

Calculation of log-normal distribution parameters from SAXS data follows the method of Harkness, et. al. (14), but uses the forward scattering $d\Sigma(0)/d\Omega$, the integrated intensity, Q, and the Porod Radius, R_p. The forward scattering, $d\Sigma(0)/d\Omega$, is evaluated by means of the Guinier approximation (15) to the scattering at low k values:

$$\frac{d\Sigma(k)}{d\Omega} = \frac{d\Sigma(0)}{d\Omega} \exp - (R_g k)^2 / 3 \qquad (3)$$

Thus, plotting the natural logarithm of the scattering intensity against k^2 yields a linear region of slope $-(R_g)^2/3$, where R_g is known as the Guinier Radius. This method of obtaining $d\Sigma(0)/d\Omega$ is shown in Fig. 5. The integrated intensity, Q, is given by the integral

$$Q = \int_0^\infty k^2 \frac{d\Sigma(k)}{d\Omega} dk \qquad (4)$$

At small values of k, the Guinier approximation is used to obtain $d\Sigma(k)/d\Omega$, while at larger values of k, the Porod Constant, P, is evaluated:

$$P = \lim_{k \to \infty} [k^4 \frac{d\Sigma(k)}{d\Omega}] \qquad (5)$$

Thus, the scattering intensity follows a k^{-4} dependence at large scattering angles. This dependence is indicated in Fig. 1. Porod's Constant is determined graphically by plotting $k^4 d\Sigma(k)/d\Omega$ as a function

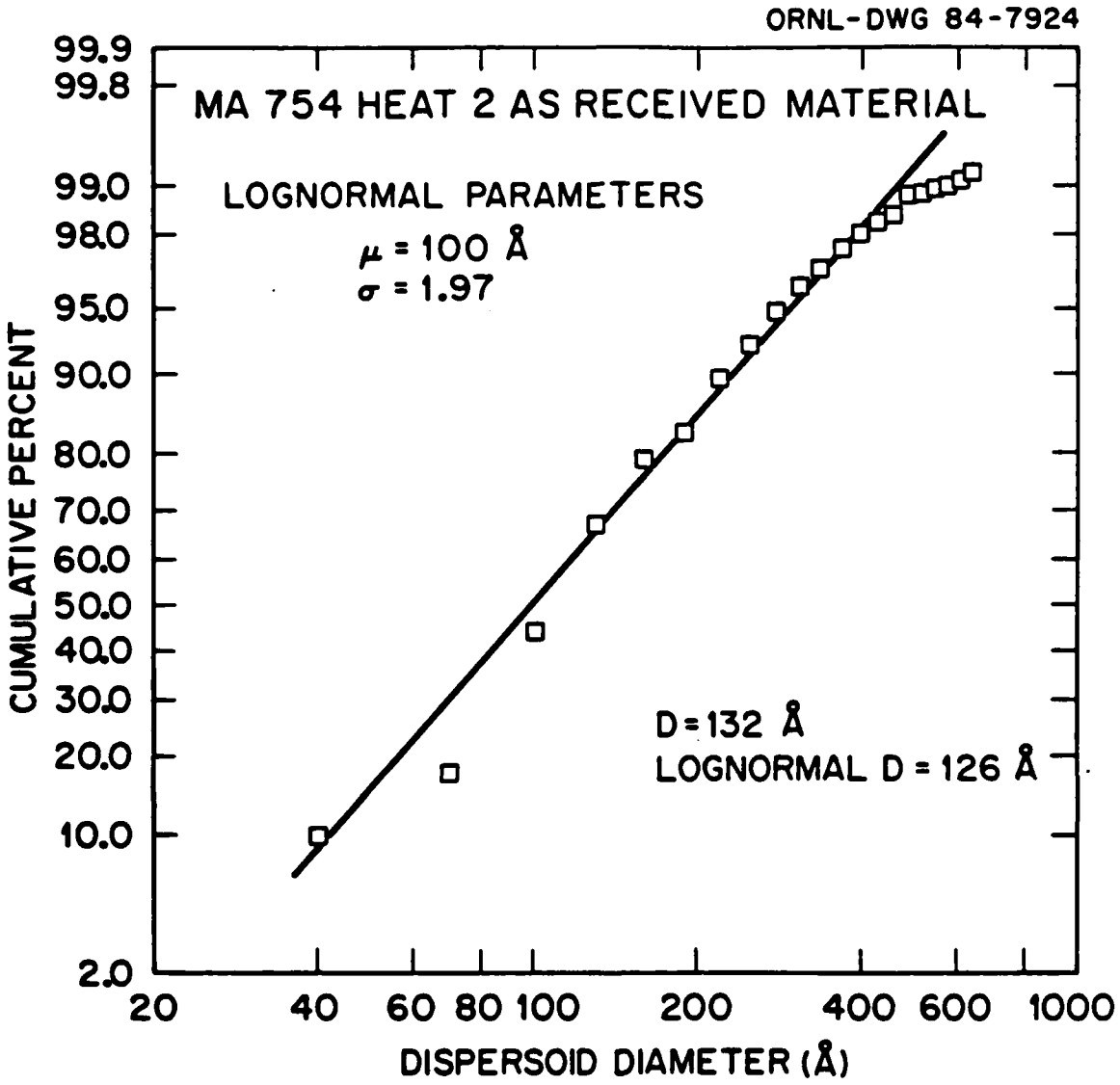

Figure 4. Cumulative probability plot of MA 754 Heat 2 AR TEM dispersoid size distribution. The solid line indicates the best fit log-normal distribution for the TEM data.

c

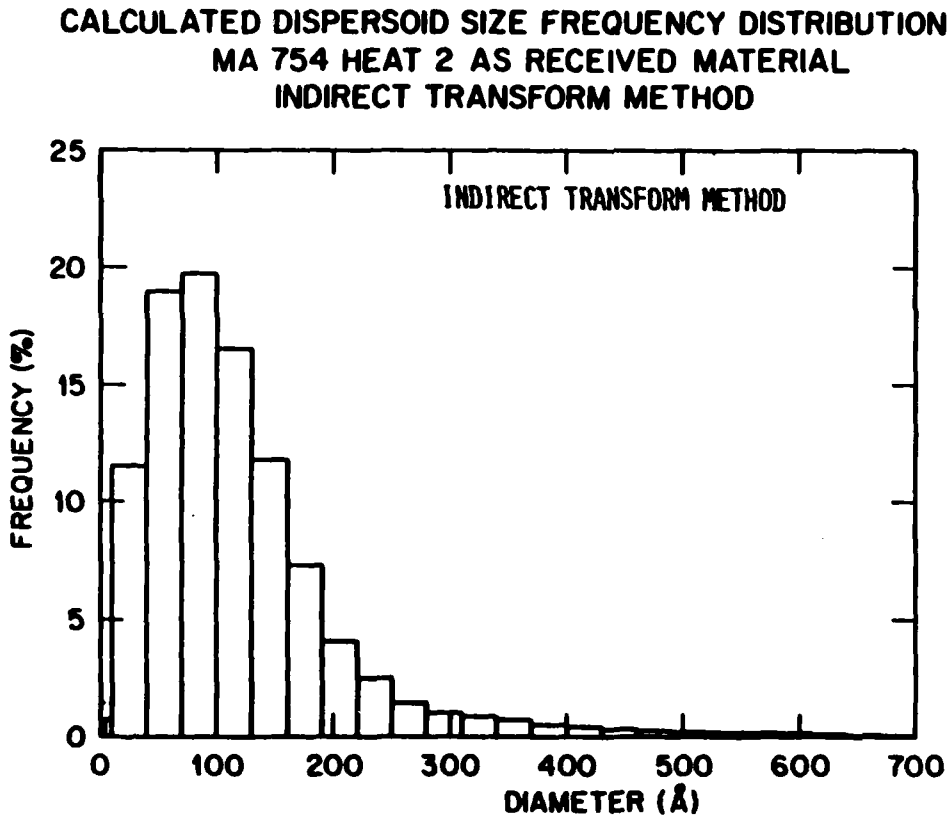

Figure 3. Dispersoid size histograms for MA 754 Heat 2 AR. (a). TEM data. (b). Calculated from SAXS log-normal analysis. (c). Calculated from indirect transform method.

b

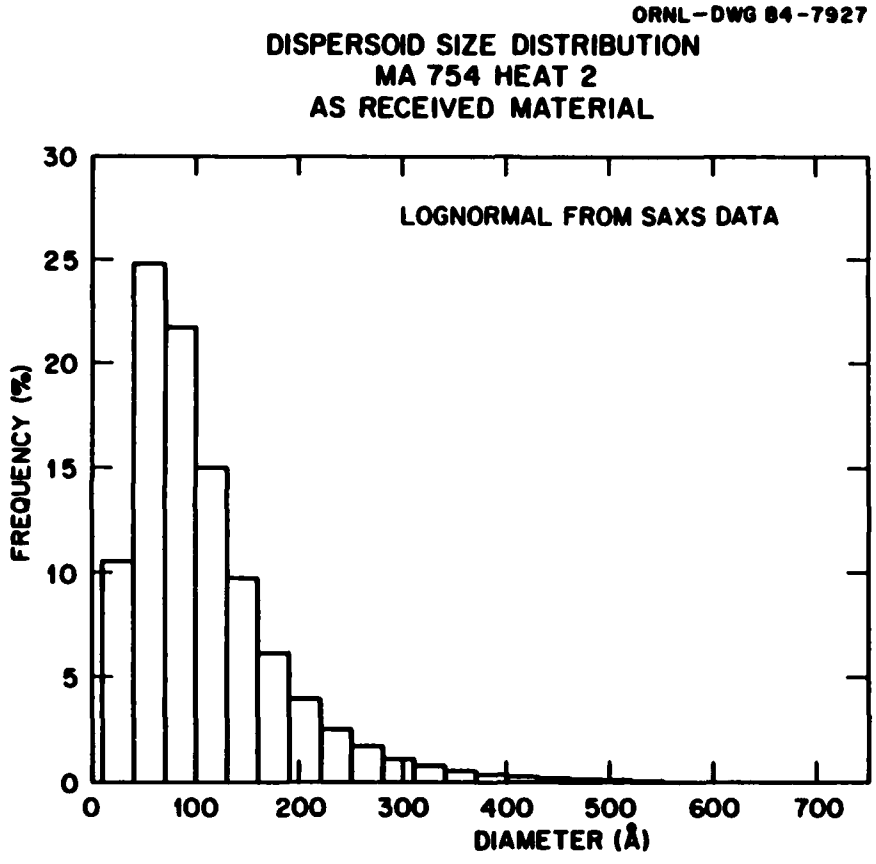

Figure 3. Dispersoid size histograms for MA 754 Heat 2 AR. (a). TEM data. (b). Calculated from SAXS log-normal analysis. (c). Calculated from indirect transform method.

a

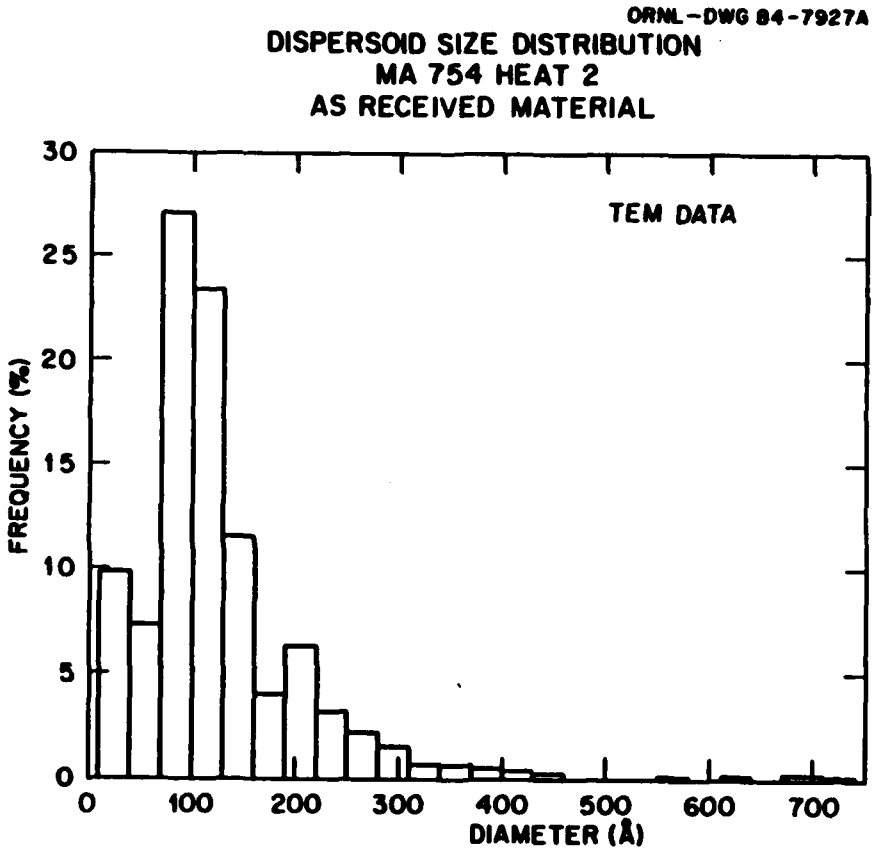

Figure 3. Dispersoid size histograms for MA 754 Heat 2 AR. (a). TEM data. (b). Calculated from SAXS log-normal analysis. (c). Calculated from indirect transform method.

transmission were recorded.

Histograms for the three conditions examined were constructed by measuring the dispersoid diameters directly from enlarged prints. An HP 9111A graphics tablet was used, and 2000 diameters were measured for each specimen condition. For each condition negatives were chosen from all of the foils which were examined. The dispersoid sizes ranged from 30 Å to approximately 1000 Å.

3. Calculation of Dispersoid Size Distributions

Before proceeding with the calculation of dispersoid size distributions from the SAXS data, it is useful to examine the TEM data to observe the qualitative trend of the dispersoid size distribution. The distribution of diameters in histogram form for Heat 2 AR, shown in Fig. 3a, has a sharp peak in the diameter range between 70 and 100 Å. The shape of the histogram - sharp rise at small diameters followed by a long decay - indicates that the log-normal distribution function (13)

$$N(D) = \frac{1}{\sqrt{2\pi}\, D \ln \sigma} \exp -\frac{1}{2}\left[\frac{\ln \mu/D}{\ln \sigma}\right]^2 \qquad (2)$$

where D is the diameter, μ is the geometric mean and σ the variance may be a good first order representation of the size distribution. In order to verify this, the data from the histogram in Fig. 3a are plotted in Fig. 4 in log-probability form, ie, the cumulative distribution is plotted as a function of the logarithm of the dispersoid diameter. The line drawn in Fig. 4 is a best fit log-normal distribution of the data. The results of log-normal analysis of the TEM data are shown in Table

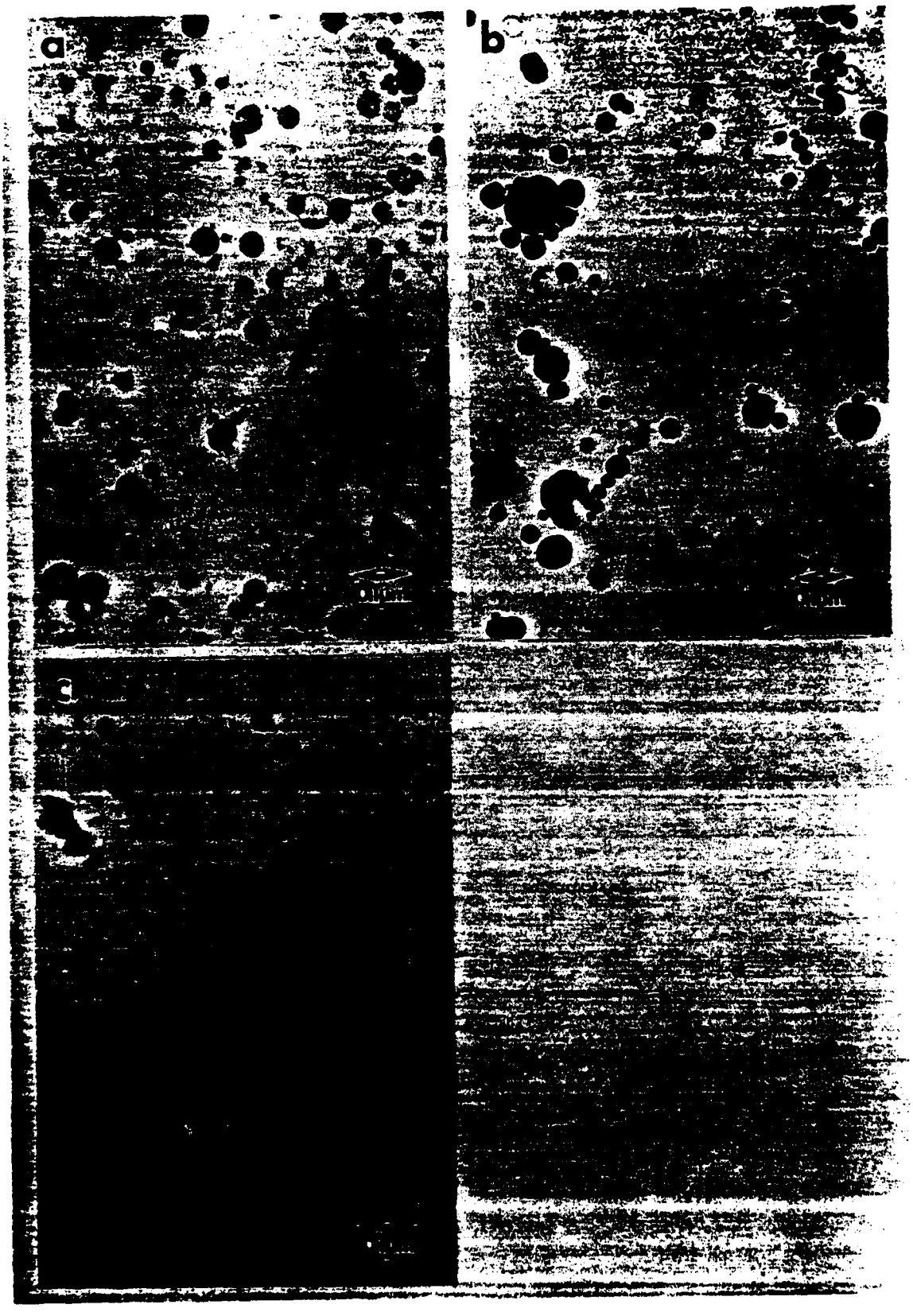

Figure 2. Typical transmission electron micrographs for the three MA 754 conditions investigated. (a). Heat 1 AR. (b). Heat 1 Ann. (c). Heat 2 AR.

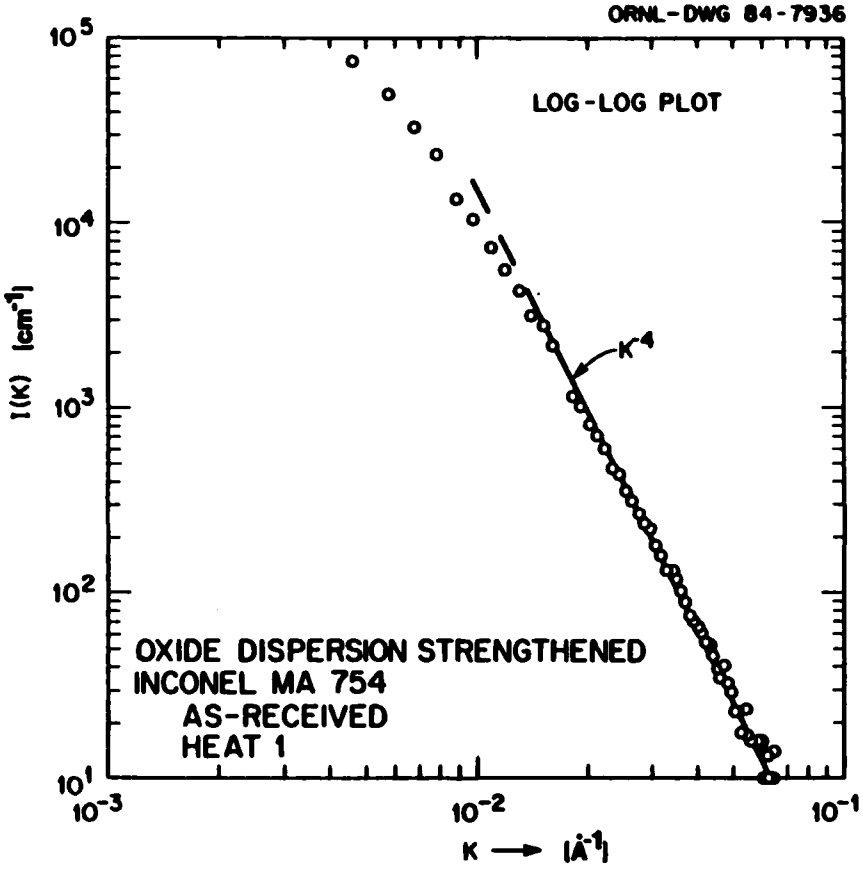

Figure 1. Dispersoid scattering cross section as a function of k vector for MA 754 Heat 1 AR.

Ray standard was cut, had been determined by neutron small angle scattering, and thereby permitted calibration of the forward scattering intensity for both experimental geometries.

The total scattering cross section, $d\Sigma(k)'/d\Omega$, is the sum of the scattering due to the dispersoids as well as the volume scattering of the nickel-chromium matrix of MA 754 (12). The scattering intensity of the matrix, $(d\Sigma(k)/d\Omega)_{NiCr}$, was measured using a nichrome specimen of composition listed in Table I. The nichrome specimen was determined to be free of second phase particles using TEM. The dispersoid scattering cross section is thus calculated from

$$\frac{d\Sigma(k)}{d\Omega} = \frac{d\Sigma'(k)}{d\Omega} - \left(\frac{d\Sigma(k)}{d\Omega}\right)_{NiCr} \qquad (1)$$

Data sets from the two beam stop runs were combined to give the dispersoid scattering cross section for a given MA 754 specimen. The dispersoid scattering cross section as a function of k for Heat 1 AR is shown in Fig. 1.

A TEM investigation was also conducted to determine the dispersoid morphology and to obtain a qualitative estimate of the dispersoid size distribution. Typical micrographs for the three specimen conditions are shown in Fig. 2. The dispersoid shape was found to be spherical by means of tilting and observing no change in dispersoid shape. A minimum of four foils were examined for each specimen condition. In the case of the AR specimens, large amounts of thin foil were obtained and bright field micrographs were obtained using kinematic conditions. The Heat 1 Ann specimens proved difficult to thin, as coarse inclusions would drop out of the foil. The small regions of Heat 1 Ann which were thinned for

thickness before electroplolishing in a 20% Perchloric, 80% ethanol solution at 20 Volts, -20°C. The SAXS specimens were dip electropolished with a fixed cathode to anode distance of 14 mm. This procedure yielded foils 12-25 μm thickness, producing X-Ray absorption products (μt) for the CuK_α line in the range of 1-2. Thin foil TEM specimens were electropolished in a twin-jet electropolishing unit.

The SAXS experiments were conducted at the Oak Ridge National Laboratory 10 Meter X-Ray Camera, utilizing a pinhole-collimated beam. A detailed description of the facility has been given by Hendricks (10). CuK_α radiation (λ=1.542 Å) was obtained from a rotating anode generator operating at 35 ma, 35 kV, with a graphite monochrometer to eliminate CuK_β. The sample-detector distance was fixed at 5.125 meters. A 64x64 element two dimensionsal position-sensitive detector array occupying a 200x200 mm grid allowed for scattering intensity to be gathered over a reciprocal lattice vector ($k=4\pi\sin\theta/\lambda$) range of 0.003-0.08 $Å^{-1}$, where θ is half the scattering angle. In order to collect scattering data over the entire range of k values, two separate sets of scattering experiments were run. The first set used a 12.5 mm beam-stop which blocked parasitic scattering from the sample aperture and thus enabled long collection times at the largest k values. A second set of experiments were run with a 7.9 mm beam-stop and short collection times to enable data acquisition at the small k values where scattering intensity is high. The absolute scattering intensity was calibrated using the scattering from Al single crystal containing neutron irradiation-produced voids. This specimen (Al-8) had been characterized in an earlier investigation by Hendricks, et. al. (11). The forward scattering cross section of the large crystal specimen from which the X-

TABLE IV. LOGNORMAL PARAMETERS OBTAINED FROM SAXS

Specimen	μ	σ	$\langle D \rangle$
Heat 1 AR	108 Å	1.86	131 Å
Heat 2 AR	89 Å	1.90	109 Å
Heat 1 Annealed	187 Å	1.62	210 Å

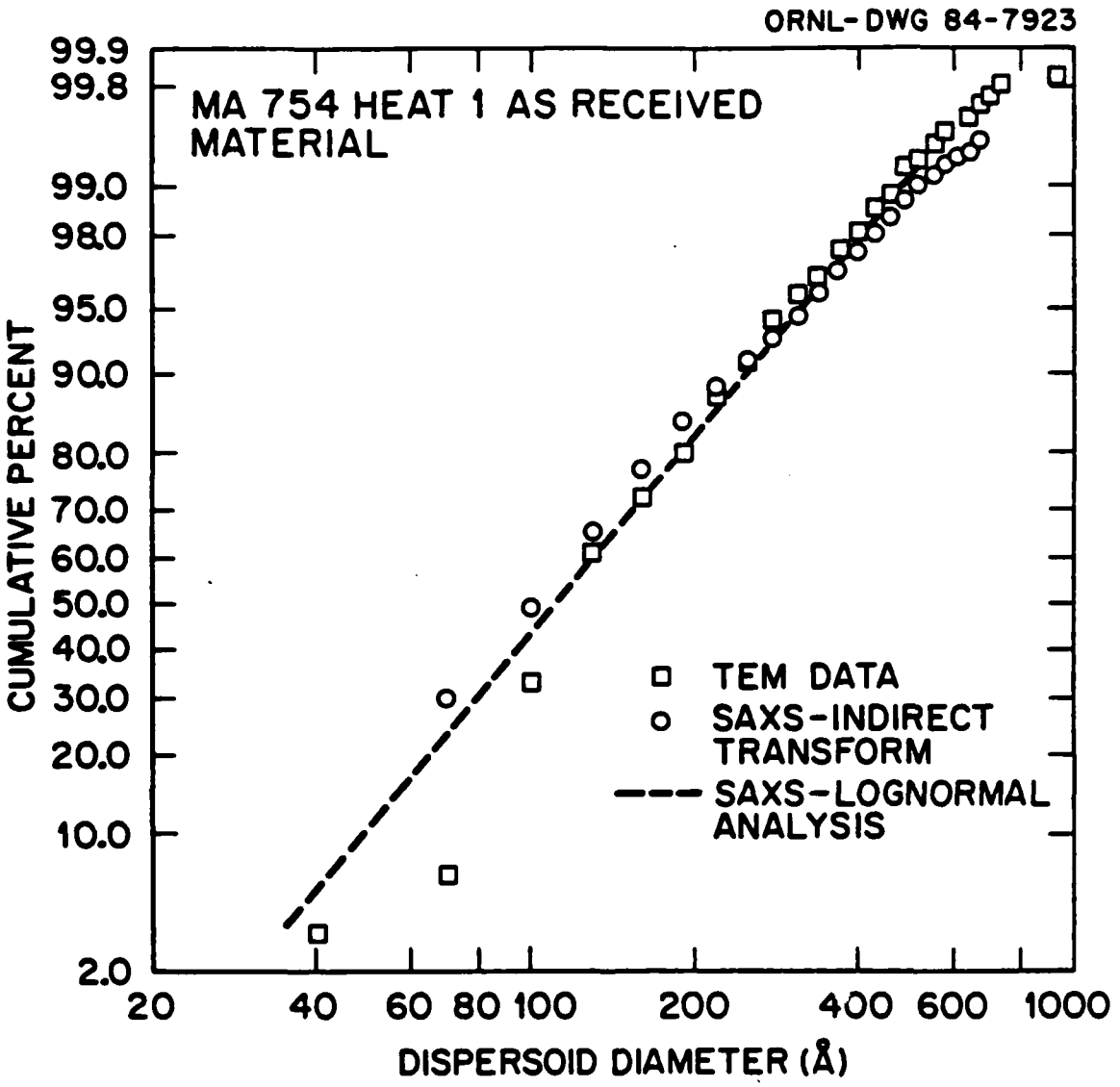

Figure 6. Cumulative probability plot of MA 754 Heat 1 AR dispersoid size distributions.

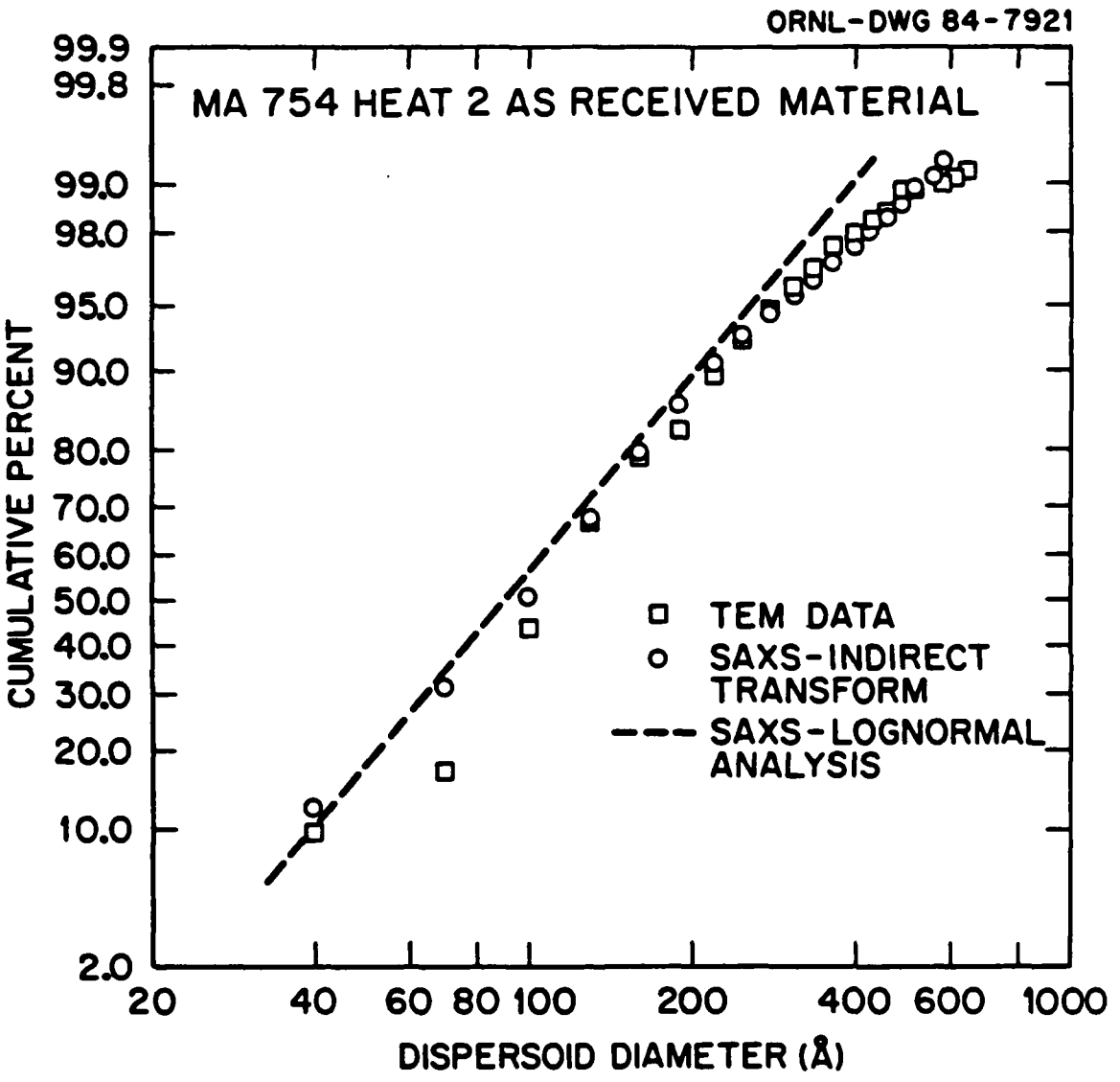

Figure 7. Cumulative probability plot of MA 754 Heat 2 AR dispersoid size distributions.

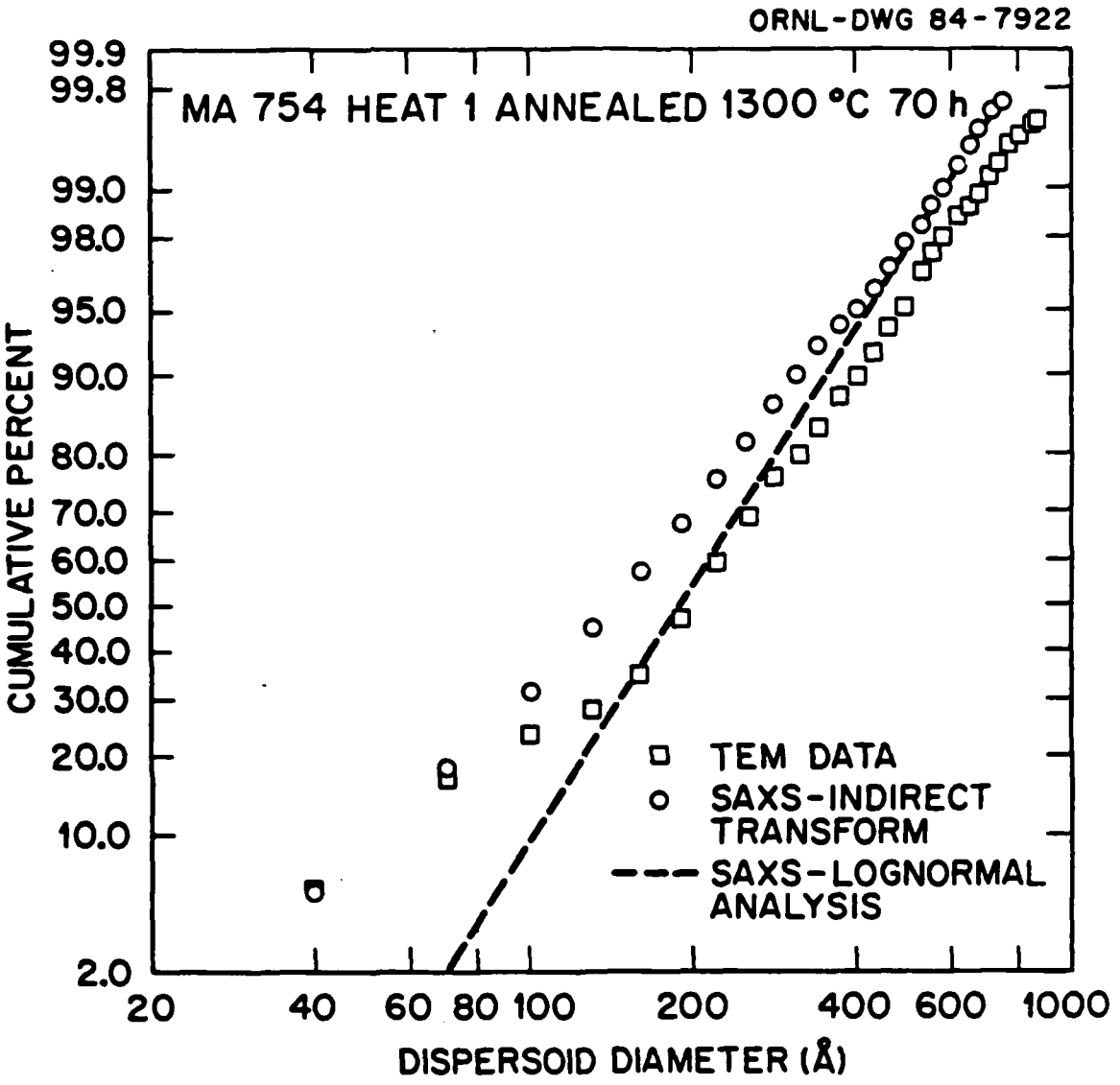

Figure 8. Cumulative probability plot of Heat 1 Ann dispersoid size distributions.

data predicts a larger frequency of dispersoids at diameters below 100 Å. The agreement between the SAXS log-normal analysis and the TEM data for Heat 1 Ann is restricted to the range of diameters between 160 and 300 Å.

A second method for determination of the dispersoid size distribution from the SAXS data is the indirect transform method originally developed by Brill, et. al. (17). The diameter distribution, for the case of identical spherical particles, is given by

$$N(D) = \frac{A}{D^2} \int_0^\infty [k^4 \frac{d\Sigma(k)}{d\Omega} - P] \; \alpha(KD) \; dk \qquad (8)$$

where

$$\alpha(x) = [(1 - 8x^{-2}) \cos x] - [(4 - 8x^{-2}) \sin x/x]$$

The advantage of the indirect transform method is that no functional form of the distribution is assumed. As in the case of the log-normal analysis, the scattering intensity must be extrapolated from k_{min} to 0 and from k_{max} to ∞.

The results of the indirect transform method for Heat 2 AR are shown in figure 9, where the log-normal distribution fit to the TEM data is shown for comparison. It is apparent that the shape of the transformed distribution function is very close to the log-normal distribution function. The cumulative distribution function is shown for Heat 2 AR in Fig. 7. Good correlation between the indirect transform distribution and the TEM data is observed at diameters of 130 Å and above. The calculated histogram for Heat 2 AR is shown in Fig. 3c. Again, as in

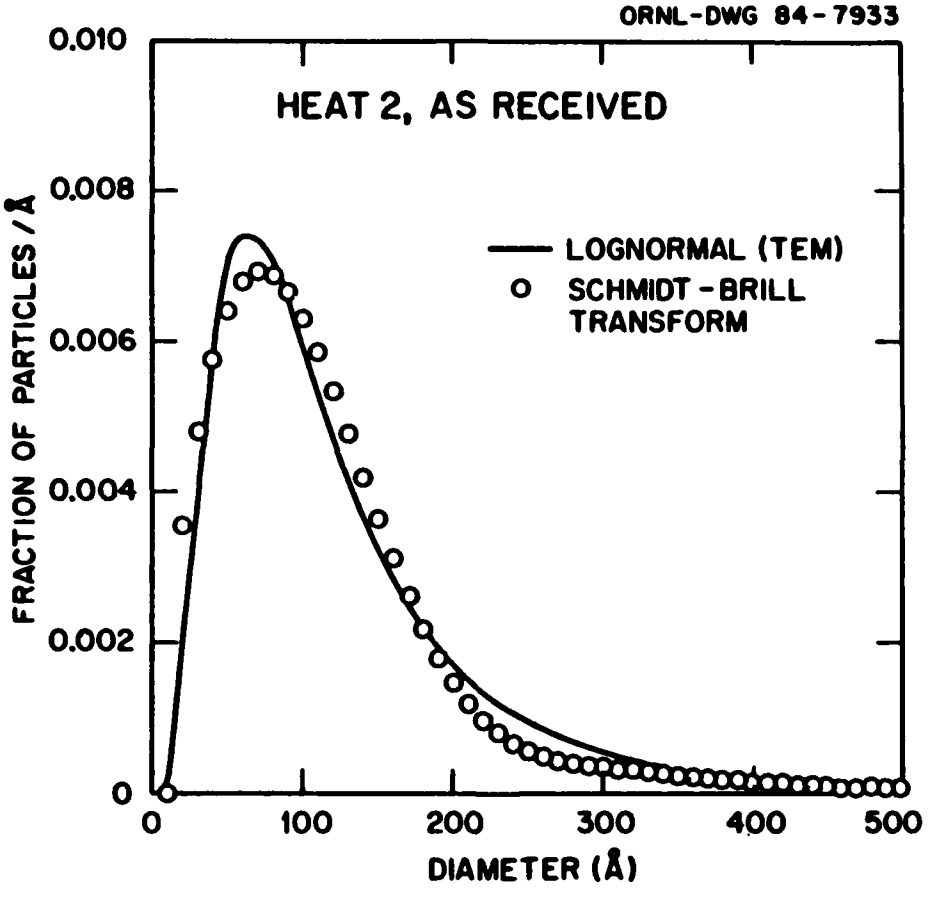

Figure 9. Dispersoid size distribution functions for MA 754 Heat 2, AR. The log-normal fit to the TEM data is compared to the dispersoid size distribution calculated using the indirect transform method.

the case of the log-normal analysis, the indirect transform method predicts a larger fraction of dispersoids at diameters less than 100 Å than the TEM data. The cumulative distribution plot of the Heat 1 AR data, shown in Fig. 6, shows overall agreement with the TEM histogram data. For the Heat 1 Ann specimen, Fig. 8, the results of the indirect transform method differ substantially from the TEM data.

The dispersoid volume fraction f present in the diameter range of dispersoids which contribute to scattering, ie, up to approximately 1000 Å, can be evaluated from the integrated intensity Q:

$$f = \frac{1}{2\pi^2} \frac{Q}{(\Delta\rho)^2} \tag{9}$$

where $(\Delta\rho)$ is the electron density difference between the dispersoids and the matrix. We use the electron density difference between Y_2O_3 and the MA 754 matrix, where $(\Delta\rho)^2=8.93 \times 10^{22} cm^{-4}$. The volume fractions for the three MA 754 conditions investigated are shown in Table V. The volume fraction of Heat 2 AR, 1.97%, is found to be 47% higher than the 1.34% measured for Heat 1 AR. This is consistent with the amount of oxygen measured in the two heats, see Table I. The volume fraction of dispersoids for Heat 1 Ann is slightly less than than of Heat 1 AR - implying that some of the dispersoids have coarsened during the course of annealing past the limit detectable by SAXS.

The number of dispersoids per unit volume, N_v, can be calculated from the volume fraction and the dispersoid size distribution. In the case of the log-normal distribution, N_v is readily calculated from the third moment of the distribution:

$$N_V = \frac{f}{\frac{\pi}{6}\langle D^3 \rangle} \tag{10}$$

Similarly, numerical integration of the indirect transform distributions is used to obtain N_v. These results are also shown in Table V.

4. Calculation of the Average Planar Dispersoid Separation Distance.

As stated above, the dislocation creep strength of a dispersion strengthened alloy depends on the magnitude of the critical shear stress, τ_c, for a dislocation to pass the dispersoids:

$$\tau_c = \frac{A G b}{\bar{L}} \tag{11}$$

where G is the shear modulus, b is the magnitude of the burgers vector, $\bar{L}$ is the average separation distance between dispersoids, and A is a constant which depends upon the specific dislocation-particle interaction examined (4-6). The relative strength of two heats of the same ODS alloy should be equal to the ratio of the respective values of τ_{c1} and τ_{c2}:

$$\frac{\tau_{c1}}{\tau_{c2}} = \frac{\bar{L}_2}{\bar{L}_1} \tag{12}$$

Thus, evaluation of $\bar{L}$ for the MA 754 specimens investigated should yield the relative creep strength of the specimens.

The calculation of $\bar{L}$ follows from a knowledge of the dispersoid size distribution and volume fraction. Following the analysis of Wilcox and Clauer (7), the average planar spacing of dispersoids, d, is given by

$$d^2 = \frac{4}{\pi N_s} \tag{13}$$

where N_s is the number of dispersoids in the plane. Fullman (18) has shown that N_s is calculated from a knowledge of the dispersoid size

TABLE V. VOLUME FRACTION f AND NUMBER OF DISPERSOIDS PER UNIT VOLUME, N_v, FROM SAXS DATA

Specimen	f	Lognormal Method N_v	Indirect Transform N_v
Heat 1 AR	1.34 %	$3.59 \times 10^{15}/cm^{-3}$	$3.11 \times 10^{15}/cm^{-3}$
Heat 2 AR	1.97 %	$8.34 \times 10^{15}/cm^{-3}$	$4.93 \times 10^{15}/cm^{-3}$
Heat 1 Annealed	1.24 %	$1.28 \times 10^{15}/cm^{-3}$	$1.72 \times 10^{15}/cm^{-3}$

distribution and volume fraction as follows:

$$N_s = \sum_i N_{si} = \sum_i \frac{6}{\pi} \frac{f_i}{D_i^2} \qquad (14)$$

In eq. (14), D_i corresponds to the average diameter of the ith size class of dispersoids, and f_i is the dispersoid volume fraction of the ith class of particles. The average planar separation distance $\bar{L}$ is obtained from the average planar spacing d by subtracting D_s, the mean diameter of intersection of a spherical particle with a random plane. It can be shown (19) that D_s is equal to $\sqrt{\frac{2}{3}}$ of the spherical diameter, while for a distribution of particle sizes the linear average of D_s will be propotional to $\langle D \rangle$ in the same amount. Thus, the average planar dispersoid spacing is given by

$$\bar{L} = d - \sqrt{2/3}\,\langle D \rangle \qquad (15)$$

or, using eqs. (13) and (14),

$$\bar{L} = \left(\frac{2}{3} \frac{1}{\sum_i f_i / D_i^2} \right)^{1/2} - \sqrt{2/3}\,\langle D \rangle$$

Using eq. (16), values of $\bar{L}$ were calculated from the SAXS derived volume fractions and dispersoid size distributions. The results of this calculation are shown in Table VI for the three MA 754 specimens considered. It is interesting to note how the value of d varies as a function of the maximum dispersoid diameter, D_{max}, included in the calculation. This variation is shown in Fig. 10 for Heat 2 AR where the dispersoid size distribution obtained from the integral transform technique has been used. The cumulative volume fraction as a function of D_{max} is also shown, and it is apparent that although dispersoid

TABLE VI. RESULTS OF CALCULATION OF AVG. PLANAR DISPERSOID SEPARATION DISTANCE, $\bar{L}$

Specimen	Indirect Transform $\bar{L}$	Lognormal Method $\bar{L}$
Heat 1 AR	1748 Å	1500 Å
Heat 2 AR	1385 Å	1069 Å
Heat 1 Annealed	1980 Å	2155 Å

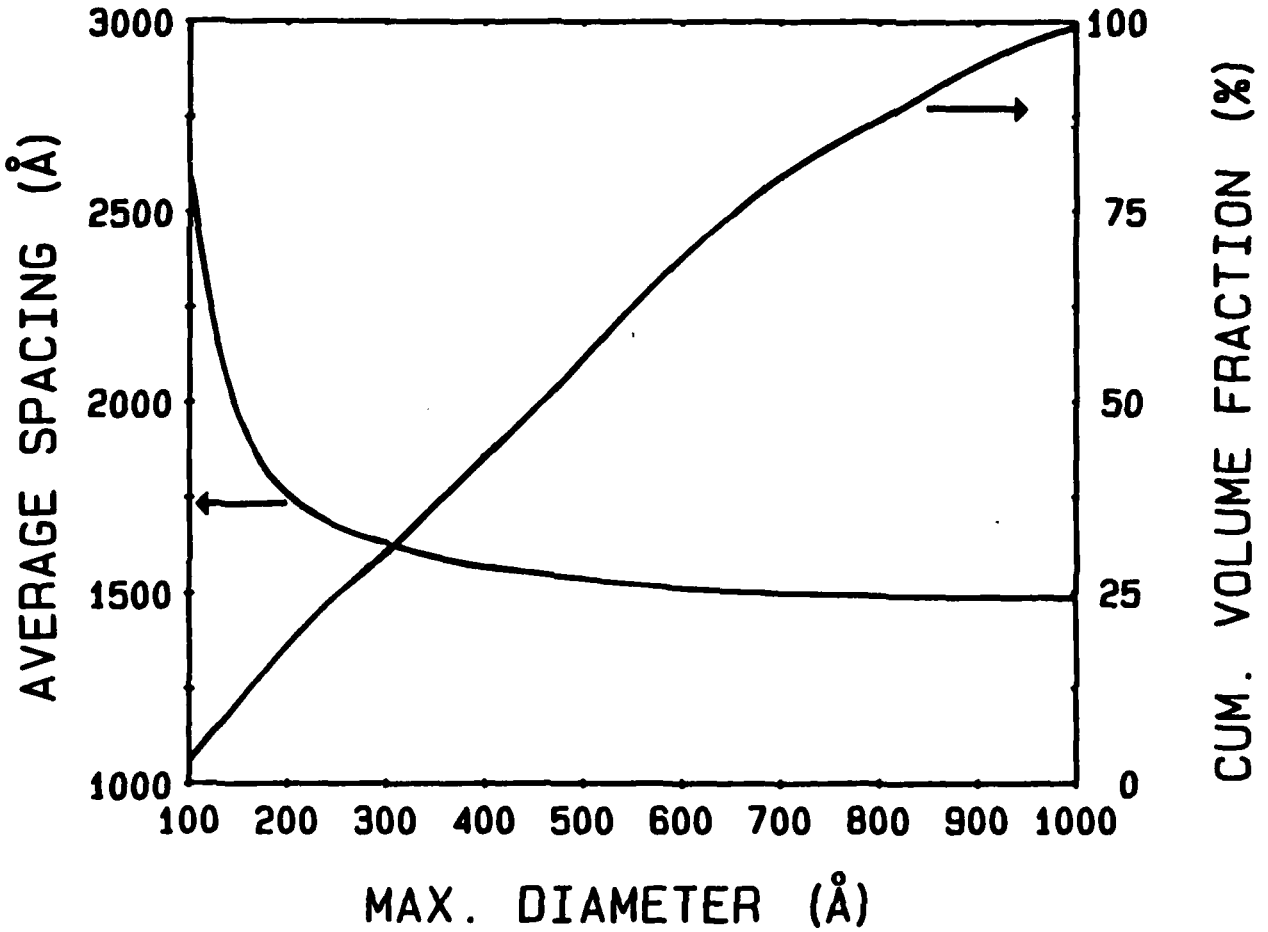

Figure 10. Average planar dispersoid spacing, d, and cumulative dispersoid volume fraction plotted as a function of D_{max}, the maximum or cutoff diameter used to calculate d. MA 754, Heat 2 AR.

diameters greater than 500 Å occupy roughly half the volume fraction, they do not contribute to reducing the average planar spacing of dispersoids. The average planar spacing, d, is within 5% of its asymptotic value in Heat 2 AR by the time D_{max} is equal to 400 Å.

5. Discussion of Results

Inspection of the results of the calculation of $\bar{L}$ in Table VI indicates that for AR MA 754, Heat 2 should have greater creep strength than Heat 1, since $\bar{L}$ for Heat 2 AR is less than $\bar{L}$ for Heat 1 AR. The strength increase for Heat 2 relative to Heat 1 from the calculated values of L is 26% using the indirect transform method, and 40% using the log-normal analysis. The longitudinal creep properties of these two heats have been determined (9,20) as part of an investigation of the elevated temperature creep properties of MA 754. The 1000°C minimum creep rate as a function of applied stress for the two heats in the as-received condition is plotted in Fig. 11. Both heats exhibit stress exponents at high stresses comparable to stress exponents measured for single crystal TDNiCr (21), while at lower stresses Heat 1 exhibits a stress exponent of 14 attributed to cavitation constrained by power law creep (9). The relative dislocation creep strength of the two heats is obtained by examining the relative strengths at a high minimum strain rate. Heat 1 requires a stress of 152 MPa to produce a minimum creep rate of $10^{-5}sec^{-1}$ at 1000°C, while Heat 2 requires 188 MPa. This corresponds to a measured strength increment of 25% for Heat 2 when compared to Heat 1. Creep data at 1093°C (9,20) reveal a 24% strength increment for Heat 2 over Heat 1. The measured strength increments

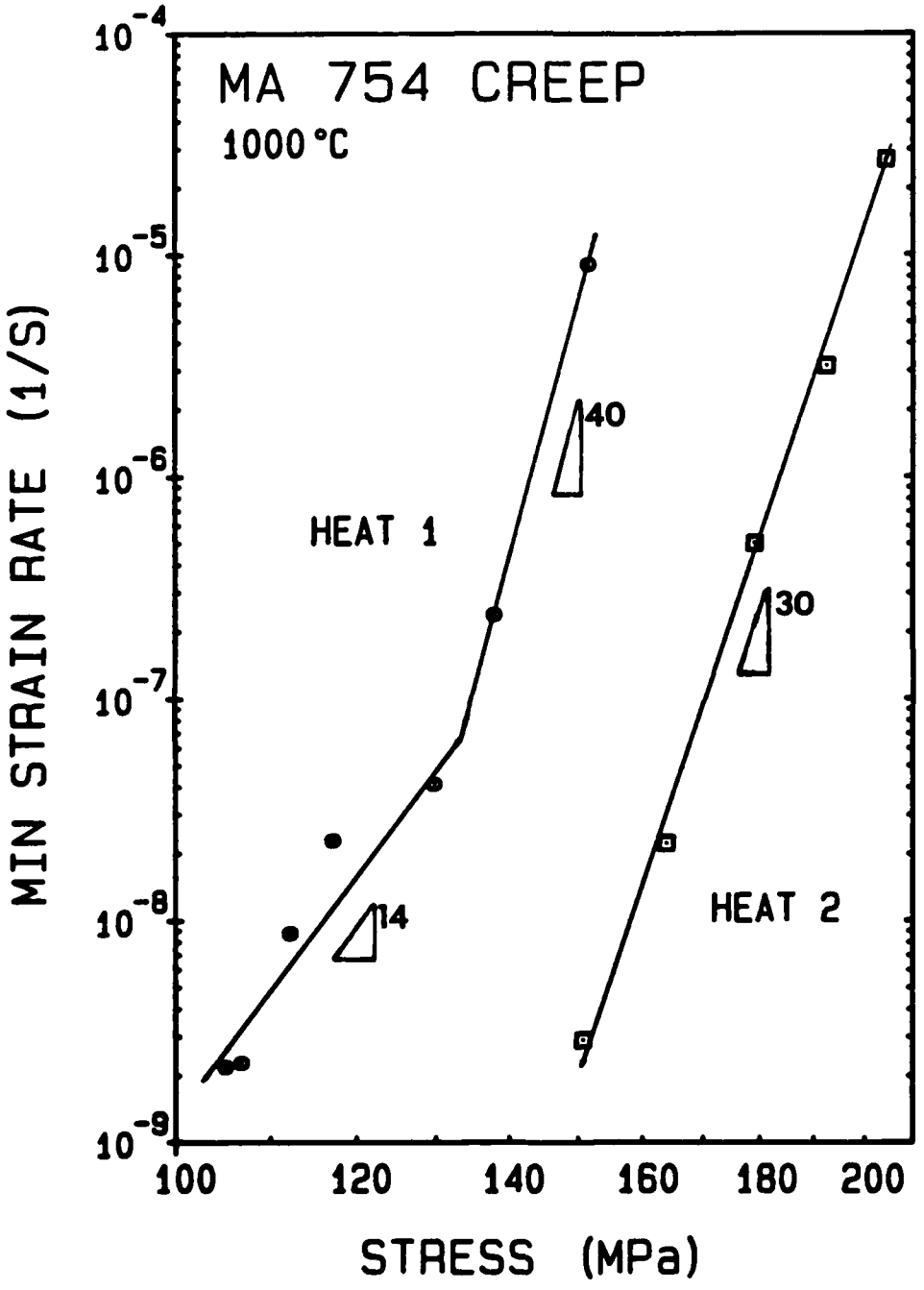

Figure 11. Constant stress creep data (9,20) for as-received MA 754 at 1000°C.

stress exponent occurs at elevated temperatures. Since the material being tested is extremely fine grained, this apparent reduction in stress exponent suggests that superplastic deformation may be possible in this alloy. To check this possibility, several constant crosshead speed tension tests were performed on the Al-8.4Fe-3.6Ce alloy at 823 K. Just as in the case of compression tests conducted at 723 K, a stress exponent of about 7.4 was observed. Furthermore, under no circumstances did the total elongation observed during tensile testing at 823 K exceed 50%. Thus, even though the limited elevated temperature compression data suggests that a change in deformation mechanism may occur at high test temperatures, tension tests at 823 K clearly show that no change in stress exponent and hence no change in deformation mechanism occurs.

A third possible explanation for the apparent loss of strength of AlFeCe at elevated temperatures is that significant microstructural coarsening may occur during elevated temperature exposure. To test this hypothesis, a thin foil TEM specimen was prepared from the as-extruded material and then heated at 773 K for 100 minutes inside the microscope. As can be seen in Figure 3, the grain size of the as-extruded material is quite fine, of the order of 0.5 μm. Furthermore, it is apparent that the distribution of second phase particles is quite heterogeneous. Regions of extremely fine (≈200 A^{o}) precipitates, such as the one shown in the center of Figure 3, are frequently observed

respectively, for pure aluminum. Note that at test temperatures below 723 K, AlFeCe is considerably stronger than ODS aluminum and exhibits a stress exponent in the range of 8 to 24. Above 723 K however, the AlFeCe alloy is substantially weaker than ODS aluminum and the limited high temperature compression data suggest that a reduction in stress exponent may be observed at elevated temperatures.

III. Discussion

As mentioned earlier, one of the primary goals of this study has been to identify and understand the factors that limit the high temperature strength of Al-8.4Fe-3.6Ce. In particular, we have attempted to understand why it has not been possible to correctly normalize the stress-strain data for this alloy. Naturally, normalization of steady state flow stress - strain rate data for an AlFeCe alloy will not be exact if the values of the lattice diffusion coefficient and the Young's modulus used in the normalization are those for pure aluminum. However, it is unlikely that the error involved in this type of normalization is large enough to account for the order of magnitude discrepancy in σ/E values observed in Figure 2.

Another possible explanation for our inability to successfully normalize the AlFeCe data is that a change in deformation mechanism occurs at elevated temperatures. As can be seen in Figure 2, data from the 773 and 823 K compression tests appear to indicate that a reduction in

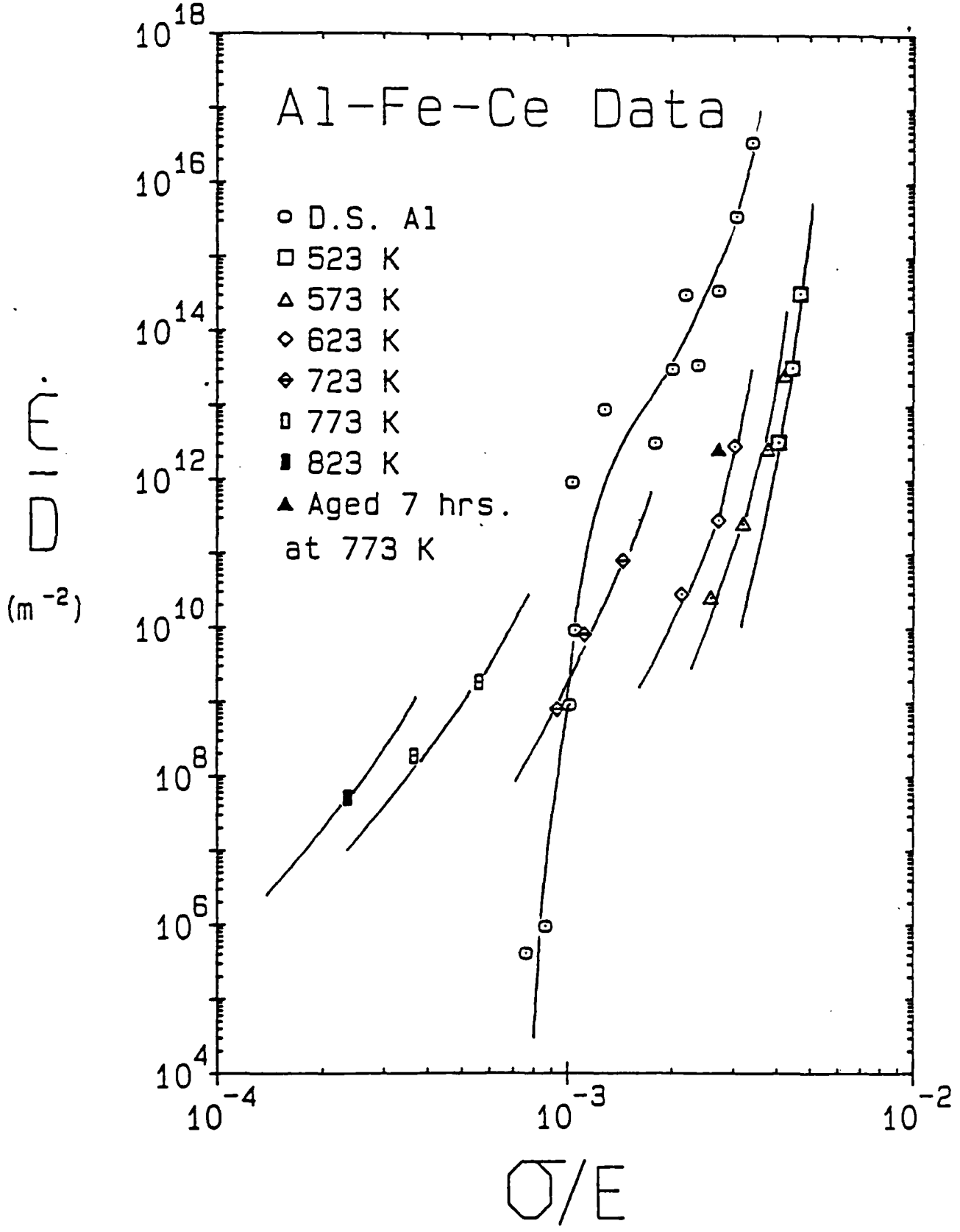

Figure 2. Temperature compensated strain rate as a function of modulus compensated stress for ODS Al and Al-8.4Fe-3.6Ce. The diffusion coefficient D is that for lattice diffusion of pure Al. The modulus, E is also for pure Al.

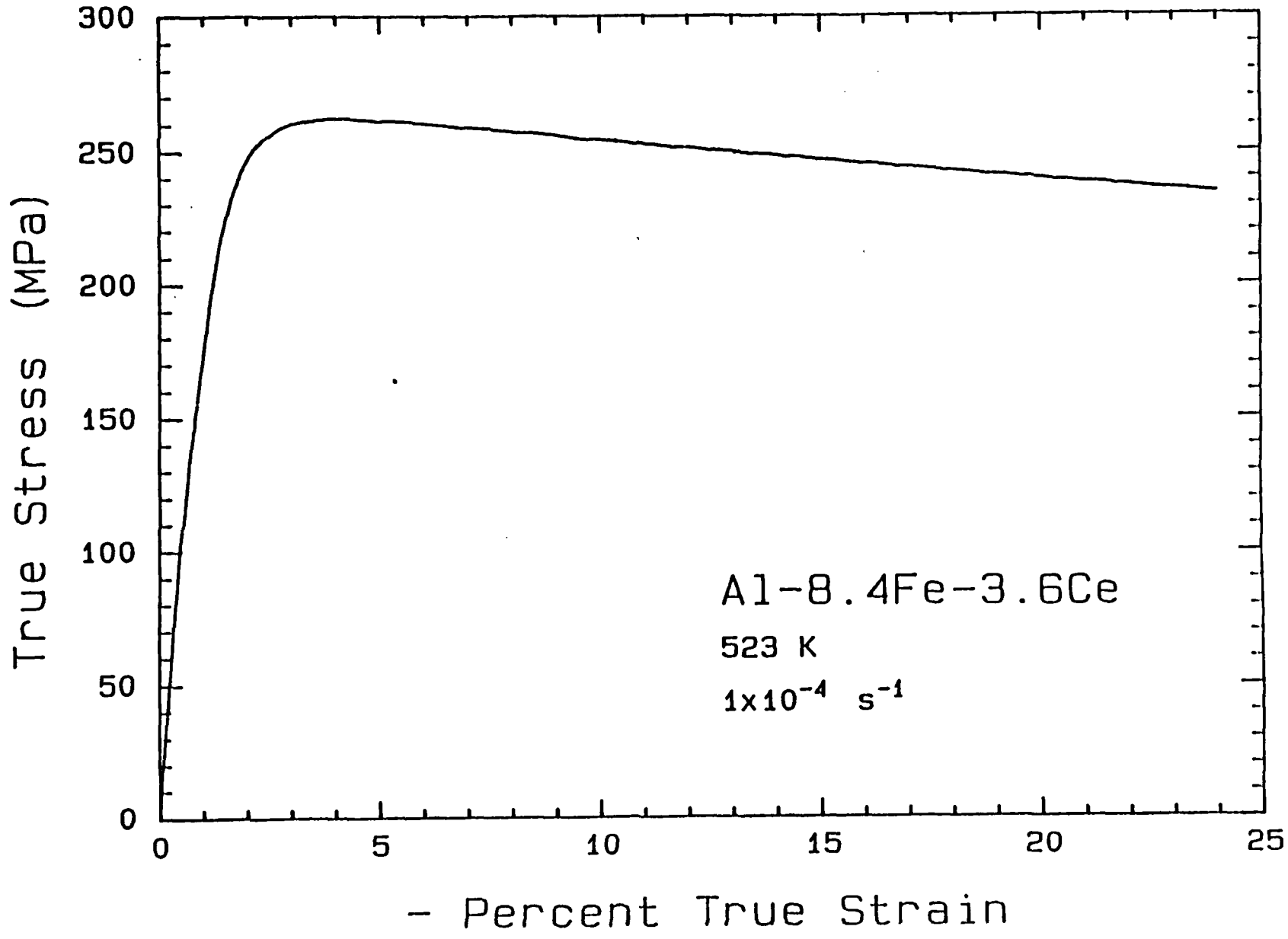

Figure 1. Typical stress-strain curve for Al-8.4Fe-3.6Ce.

B.

MICROSTRUCTURAL CHANGES ASSOCIATED WITH ELEVATED TEMPERATURE DEFORMATION IN Al-8.4Fe-3.6Ce

I. Introduction

During the past year we have studied the high temperature deformation behavior of fine grained Al-8.4$^{w}/_{o}$Fe-3.6$^{w}/_{o}$Ce. In particular, we have attempted to understand the factors that limit the strength of this material at elevated temperatures (>723 K). The compressive flow properties of this AlFeCe alloy have been examined and transmission electron microscopy (TEM) has been used to examine the microstructural changes associated with elevated temperature deformation and exposure.

II. Results

Constant true strain rate compression tests were performed at strain rates varying from 10^{-6} to 10^{-3} sec^{-1} using an Instron electromechanical testing machine in conjunction with a Hewlett-Packard data acquisition and control system. Test temperatures ranged from 523 to 803 K. A typical stress-strain curve is shown in Figure 1. Note that as in all tests, strain softening is readily observed. Figure 2 shows the combined results of all compression tests with data from compression tests of oxide dispersion strengthened (ODS) aluminum (Ref. 1) included for comparison. Strain rates and stresses are normalized by the lattice diffusion coefficient and elastic modulus,

We then solve for $\ln \mu$ and $\ln^2 \sigma$, yielding

$$\ln \mu = 2.25 \ln (2 R_p) - \frac{1}{2.4} \ln \left(\frac{12 \pi \ d\Sigma(0)/d\Omega}{Q}\right) \quad \text{(A8)}$$

$$\ln^2 \sigma = \frac{1}{6} \ln \left(\frac{12 \pi \ d\Sigma(0)/d\Omega}{Q}\right) - \frac{1}{2} \ln (2 R_p) \quad \text{(A9)}$$

It should be emphasized that eqs. (A8) and (A9) are constructed from the ratios $\langle D^6 \rangle / \langle D^3 \rangle$ and $\langle D^3 \rangle / \langle D^2 \rangle$. Calculation of μ and σ from other moment ratios are possible. For example, R_g in a point-collimated experiment is equal to $0.25 \langle D^8 \rangle / \langle D^6 \rangle$. Harkness, et. al. (14) use R_p and R_g to obtain log-normal distribution parameters. However, they were dealing with log-normal distributions of small variances, characteristic of GP zones in Al Alloys. For the case of a polydisperse distribution of diameters such as MA 754, the errors in determination of the parameters are minimized by choosing to extract μ and σ from ratios of the lower order moments of the size distribution.

where $\Delta\rho$ is the difference in electron density between the dispersoid and matrix, N_V is the number of dispersoids per unit volume, and D is the dispersoid diameter. The integrated intensity, Q, is related to the third moment of the size distribution

$$Q = \frac{\pi^3}{3} (\Delta\rho)^2 N_V \langle D^3 \rangle \tag{A2}$$

The Porod Constant, P, is related to the average surface area of dispersoids, ie, the second moment of the size distribution:

$$P = 2 \pi^2 (\Delta\rho)^2 N_V \langle D^2 \rangle \tag{A3}$$

From eqs. (A2) and (A3) we find that the Porod Radius R_p is proportional to the ratio $\langle D^3 \rangle / \langle D^2 \rangle$:

$$R_p = \frac{3}{\pi} \frac{Q}{P} = \frac{1}{2} \frac{\langle D^3 \rangle}{\langle D^2 \rangle} \tag{A4}$$

For the log-normal distribution, the nth moment $\langle D^n \rangle$ can be written as (13)

$$\langle D^n \rangle = \exp (n \ln \mu + \frac{1}{2} n^2 \ln^2 \sigma) \tag{A5}$$

This expression permits one to write simple expressions for ratios of moments of the log-normal distribution in terms of the geometric mean μ and variance σ.

We construct the ratio $\langle D^6 \rangle / \langle D^3 \rangle$ from eqs. (A1) and (A2):

$$\frac{\langle D^6 \rangle}{\langle D^3 \rangle} = \frac{12 \pi \, d\Sigma(0)/d\Omega}{Q} = \exp (3 \ln \mu + 13.5 \ln^2 \sigma) \tag{A6}$$

Using eq. (A4) we obtain an expression for R_p in terms of μ and σ

$$R_p = \frac{1}{2} \exp (\ln \mu + \frac{5}{2} \ln^2 \sigma) \tag{A7}$$

(18) R.L. Fullman. Trans. A.I.M.E. 197 , 447 (1953).

(19) J.W. Martin. Micromechanisms in Particle Hardened Alloys Cambridge: Cambridge University Press, 1980. p. 44.

(20) J.J. Stephens. Unpublished research. Stanford University, 1983.

(21) R.W. Lund, W.D. Nix. Acta Metall. 24 ,469 (1976).

(22) M. Raghavan, C. Klein, R. Petkovic-Luton. Proceedings of the Thirty-Ninth EMSA Meeting Atlanta, 1981. p. 142.

(23) J.S. Benjamin, T.E. Volin. High Temperatures, High Pressures 6 , 443 (1974).

(24) T.A. Ramanaryanan, R. Petkovic-Luton, R. Ayer. "Alumina-Yttria Mixed Oxides in Dispersion Strengthened High Temperature Alloys". U.S. Patent #4,402,746. Sept. 6, 1983.

Appendix

Calculation of Log-Normal Distribution Parameters from SAXS Data

Calculation of the log-normal distribution parameters from SAXS data is reasonably straigtforward since SAXS parameters such as the forward scattering $d\Sigma(0)/d\Omega$, integrated intensity Q, and Porod Constant P represent moments of the size distribution of dispersoids in the specimen (11). Harkness, et. al. (14) have derived expressions for extracting log-normal parameters from slit-collimated SAXS data. We derive expressions for the case of point collimated SAXS data, appropriate to our experimental conditions. The dispersoids are assumed to be spherical, and only one type of dispersoid is assumed present.

The forward scattering, $d\Sigma(0)/d\Omega$, is proportional to the sixth moment of the size distribution:

$$\frac{d\Sigma(0)}{d\Omega} = (\Delta\rho)^2 \; N_V \frac{\pi^2}{36} \; \langle D^6 \rangle \qquad \text{(A1)}$$

this manuscript. One of the authors (JJS) was supported by the Air Force Office of Scientific Research, Contract AFOSR 81-0022C.

References

(1) B.A. Wilcox, A.H. Clauer. Acta Metall. 20 ,743 (1972).

(2) J.S. Benjamin. Met. Trans. 1 ,2943 (1970).

(3) W. Crawford. "Oxide Dispersion Strengthened Materials in Advanced Gas Turbine Engines - MA 754 Vanes", J.S. Benjamin, ed., Frontiers of High Temperature Materials II , INCO MAP, 1983.

(4) A.J.E. Forman, M.J. Makin. Phil. Mag. 13 , 911 (1966).

(5) U.F. Kocks. Phil. Mag. 13 , 541 (1966).

(6) D.J. Srolovitz, R.A. Petkovic-Luton, M.J. Luton. Acta Metall. 31 , 2151 (1983).

(7) B.A. Wilcox, A.H. Clauer. Trans. A.I.M.E. 236 , 570 (1966).

(8) S.M. Allen. Phil. Mag. A 43 ,325 (1981). 6 , 443 (1974).

(9) J.J. Stephens, W.D. Nix. "Creep and Fracture of Inconel MA 754 at Elevated Temperatures" in M. Gell, (ed.); Proceedings of the Fifth International Symposium on Superalloys A.I.M.E., 1984.

(10) R.W. Hendricks. J. App. Cryst. 11 , 15 (1978).

(11) R.W. Hendricks, J. Schelten, W. Schmatz. Phil. Mag. 30 , 819 (1974).

(12) V. Gerold. "Application of Small Angle X-Ray Scattering to Problems in Physical Metallurgy and Metal Physics" in H. Brumberger, ed.; Small Angle X-Ray Scattering New York: Gordon & Breach, 1967.

(13) E.E. Underwood. Quantitative Stereology Reading, Mass.: Addison-Welsley, 1970.

(14) S.D. Harkness, R.W. Gould, J.J. Hren. Phil. Mag. 19 , 115 (1969).

(15) A. Guinier, G. Fournet. Small Angle Scattering of X-Rays New York: John Wiley & Sons, 1955.

(16) O. Glatter, O. Kratky. Small Angle X-Ray Scattering New York: Academic Press, 1982.

(17) O.L. Brill, C.G. Weil, P.W. Schmidt. Journal of Colloidal and Interface Science. 27 , 479 (1968).

contents, it is necessary (24) to start mechanical alloying with $5Al_2O_3 3Y_2O_3$ (yttrium-aluminum garnet). This procedure also minimizes the amount of aluminum lost from the matrix to the dispersoids, which is important to ensure continuous Al_2O_3 oxide formation for oxidation resistance.

Conclusions

We have seen that SAXS is a useful method for determination of dispersoid size distributions and volume fractions in the ODS alloy MA 754. The indirect transform technique is the more exact method for extracting dispersoid size distributions from the SAXS data, although the log-normal distribution function has proven to be a useful method for first order analysis in this study. Evaluation of the average planar dispersoid spacing for two heats of as-received MA 754 shows that the difference in dislocation creep strength of these two heats is consistent with the calculated dispersoid spacings. The effect of mixed oxides in MA 754 on the above results is minimal due to the fact that all the mixed oxides have scattering strengths $(\Delta\rho)^2$ similiar to that of Y_2O_3.

Acknowledgements

We would like to acknowledge the help of Dr. J. Kortright in conducting preliminary scattering experiments at Stanford Synchrotron Radiation Laboratory. Consultations with Professor W.D. Nix were valuable in shaping the scope of the investigation and the review of

oxides which are found in MA 754 are strongly scattering in the nickel-chromium matrix: $(\Delta\rho)^2$ for Y_2O_3 in MA 754 is twice as large as the scattering strength of voids in an Al matrix ($4.24 \times 10^{22} cm^{-4}$). Inspecton of Table VII shows that the oxide $AlYO_3$ has the largest deviation in $(\Delta\rho)^2$ from Y_2O_3 - it scatters 37% less strongly than Y_2O_3. This leads to an error in D of roughly 6.5%. We conclude that the error in the dispersoid size distribution due to the presence of mixed oxides is minimal, and is within the expected reproduceability limits of quantitative metallographic techniques.

It is interesting to compare the dispersoid size distributions in MA 754 to the as-calcined Y_2O_3 size distribution used in mechanical alloying. We have listed in Table II the log-normal parameters for as-calcined Y_2O_3 which are typical of the starting dispersoid powder in mechanically alloyed ODS alloys (23). During the course of mechanical alloying and 2 hr. anneal at 1315°C, the average dispersoid diameter in MA 754 increases to roughly 130 Å from the 90 Å average for as-calcined Y_2O_3. Note that the variance of the log-normal distribution for as-calcined Y_2O_3 is very similar to those observed in MA 754. The effect of annealing MA 754 for an additional 70 hrs. at 1300°C is to increase the average diameter to approximately 230 Å, given by the log-normal fit to the TEM data. By comparison, the mechanically alloyed nickel based ODS alloy IN 853 (with 1.5 wt% Al, 1.31% Y_2O_3, 0.33% Oxygen) coarsens after a 2 hr., 1315°C anneal to an average diameter of 307 Å (23). It is apparent that the low aluminum content of MA 754 serves to minimize the amount of dispersoid coarsening which occurs during the alloy processing. In order to minimize the amount of dispersoid coarsening which occurs during the processing of ODS alloys with higher aluminum

TABLE VII. SCATTERING STRENGTHS OF OXIDES IN MA 754 MATRIX

(ρ for MA 754 Matrix = $6.83 \times 10^{11} cm^{-2}$)

Oxide	Crystal Structure	ρ $(cm)^{-2}$	$(\Delta\rho)^2 (cm)^{-4}$
Y_2O_3	bcc	3.84×10^{11}	8.93×10^{22}
$5\ Al_2O_3\ 3\ Y_2O_3$	cubic	3.62×10^{11}	10.3×10^{22}
α - Al_2O_3	hexagonal	3.32×10^{11}	12.3×10^{22}
$Al_2O_3\ 2\ Y_2O_3$	monoclinic	3.52×10^{11}	10.9×10^{22}
$AlYO_3$	orthorhombic	4.24×10^{11}	6.69×10^{22}
ThO_2	fcc	6.95×10^{11}	0.014×10^{22}

used microanalytical techniques to characterize the chemical composition and crystal structure of dispersoids in the mechanically alloyed nickel based ODS alloys. They have found Al_2O_3 and mixed yttrium-aluminum oxides present in addition to Y_2O_3. The mixed oxides are found at diameters of 200 Å and above, although it is not clear whether this is a real minimum diameter or a limitation of probe diameter used for STEM microanalysis. The amount of mixed oxide formation which occurs is proportional to the amount of Al present in the master alloy: Al_2O_3 and mixed oxide formation occurs through the course of mechanical alloying and subsequent thermomechanical processing. It is necessary to evaluate the effect the presence of mixed oxides has on the dispersoid size distributions obtained for MA 754.

The absolute cross section for scattering by dispersoids, $d\Sigma(k)/d\Omega$, can be written in terms of the dispersoid size distribution in the following manner:

$$\frac{d\Sigma(k)}{d\Omega} = \int_0^\infty (\Delta\rho)^2 \; N(D) \; V^2(D) \; | \; F(k,D) \; |^2 \; dD \qquad (17)$$

where $F(k,D)$ is the geometric form factor of the dispersoid. From eq. (17) we see that given a known $d\Sigma(k)/d\Omega$ variations in $(\Delta\rho)^2$ due to different dispersoids leads to errors in $N(D)V^2(D)$. Assuming that the dispersoid size distribution is log-normal, $N(D)$ is given by eq. (2) and to first order:

$$\frac{d\Sigma(k)}{d\Omega} \propto (\Delta\rho)^2 \; D^5 \qquad (18)$$

This implies that variations in $(\Delta\rho)^2$ will lead to errors in D^5. The calculated values of $(\Delta\rho)^2$ for the oxides of interest with respect to the matrix composition of MA 754 are shown in Table VII. The value of $(\Delta\rho)^2$ for ThO_2 is also included in Table VII, showing that all of the

agree very well with the creep strength increase of 26% predicted by the indirect transform method. Thus, the values of $\bar{L}$ calculated for AR MA 754 from the indirect transform method support the idea that the dislocation creep strength of ODS alloys are governed by the average planar separation of dispersoids.

The difference in predicted relative creep strength using the two SAXS analysis methods can be understood as follows. Examination of Fig. 7 indicates that the dispersoid size distribution obtained by the SAXS log-normal analysis for Heat 2 AR diverge from the TEM and indirect transform data above 300 Å. The log-normal analysis predicts generally smaller dispersoids for this heat - that is, the log-normal trend line lies to the left of the other two size distributions. The net effect is to increase N_v given a fixed volume fraction for the log-normal analysis. This means N_s will also be larger, and therefore the calculated values of $\bar{L}$ will be smaller. Inspection of Fig. 6 reveals a similar divergence between the log-normal analysis and the indirect transform method for Heat 1 AR although the divergence occurs above 430 Å and hence there is less disagreement between the values of $\bar{L}$ obtained from the two methods for this specimen. The fact that the indirect transform method does not a priori assume a functional form of the size distribution leads us to conclude that the indirect transform method gives the closest representation of the true dispersoid size distributions in MA 754.

In order to extract the dispersoid size distributions from the SAXS data, all the dispersoids have been assumed to be identical, ie, a $(\Delta\rho)^2$ corresponding to Y_2O_3 has been used. Other investigators (22,23) have

Figure 3. TEM micrographs of Al-8.4Fe-3.6Ce: (a) in the as-extruded condition; (b) at 773 K and after 100 minutes at temperature;

Figure 3. TEM micrographs of Al-8.4Fe-3.6Ce: (c) after cooling back to room temperature.

suggesting that portions of the rapidly solidified starting material remain unchanged after extrusion. Upon heating to 773 K, particle coarsening occurs and is especially prevalent in the regions initially containing the finest precipitates. However, as can be seen in Figure 3, even after 100 minutes at 773 K, microstructural coarsening does not appear to be severe enough to account for the order of magnitude discrepancy in σ/E seen in Figure 2. In order to further confirm that only limited softening will result from microstructural coarsening in Al-8.4Fe-3.6Ce, an as-extruded specimen was annealed at 773 K for 7 hrs. (and furnace cooled to room temperature) prior to testing at 573 K. As can be seen in Figure 2, the annealed specimen is indeed somewhat softer than an identically tested as-extruded specimen however, as expected, microstructural coarsening alone is not responsible for the order of magnitude discrepancy in σ/E shown in Figure 2.

It should also be noted, with regard to the hot stage TEM experiment, that particle dissolution during elevated temperature exposure is not responsible for the observed softening. No new particles were observed to precipitate out of solution when the 100 minute, 773 K aged specimen was cooled to room temperature. Thus, a reduction in the number of particles due to dissolution is not responsible for the loss in strength observed in AlFeCe during elevated temperature deformation. Furthermore, since particle dissolution does not occur, reprecipitation of particles is

not responsible for the recovery of strength that occurs when a specimen exposed to elevated temperatures is cooled to room temperature.

One final explanation for the apparent loss of strength of AlFeCe at elevated temperatures is that the second phase particles responsible for the superior low temperature strength of the AlFeCe alloy simply become weak at high temperatures, losing their ability to serve as effective barriers to dislocation motion. In order to investigate this possibility, a sample was deformed 25% at 773 K at a strain rate of 1×10^{-5} sec^{-1}. A representative view of the tested specimen, as revealed by TEM, is shown in Figure 4. Note that as in the hot stage experiment, extremely fine particles characteristic of the rapidly solidified structure have been replaced by much larger, accicular particles. In addition, as can be seen in Figure 5, a number of particles present in the elevated temperature tested specimen exhibit an unusual fringe contrast effect. A pair of complementary bright field - dark field micrographs of one of these particles are shown in Figure 6. Contrast effects of this type are typically associated with twinning. Thus, since similar contrast effects were not observed in lower temperature tested specimens, it appears that the reduction in strength of AlFeCe alloys at elevated temperatures is due to the fact that a large number of the second phase particles deform by twinning at elevated temperatures.

Figure 4. TEM micrographs of Al-8.4Fe-3.6Ce deformed 25% at 773 K at a strain rate of 1×10^{-5} sec^{-1}. Representative view.

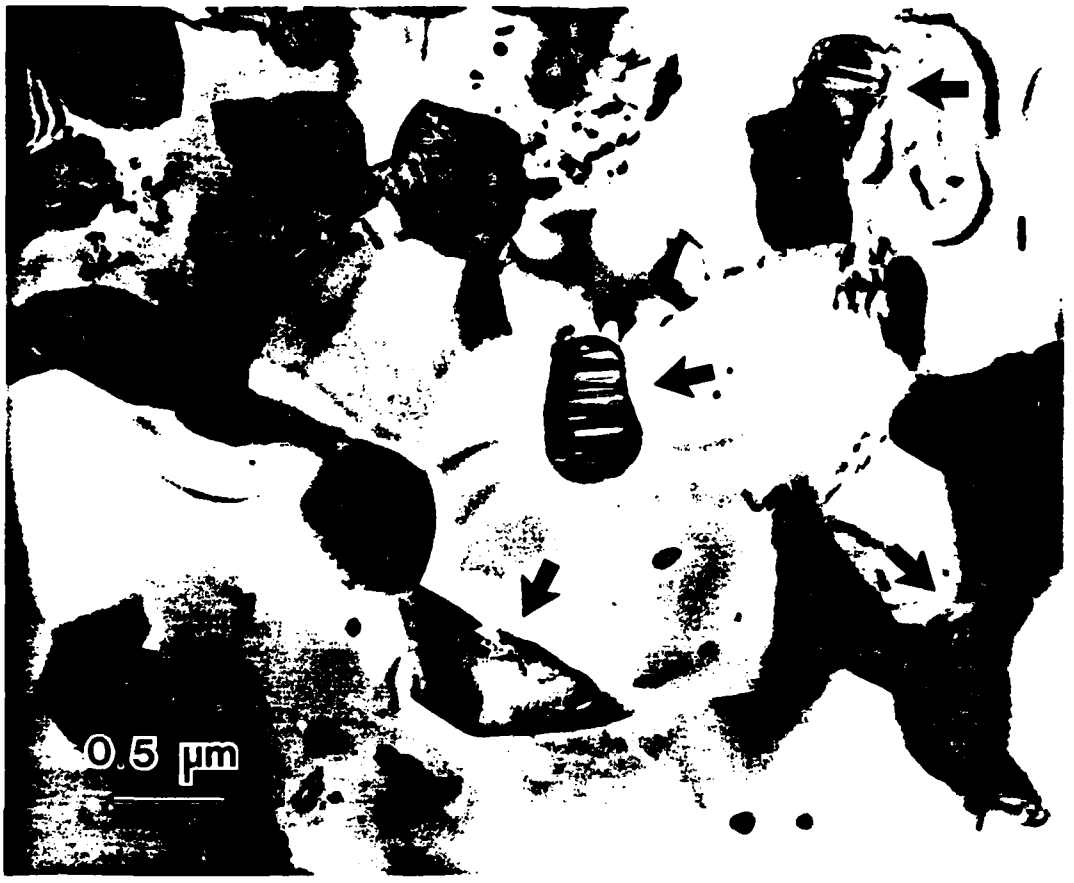

Figure 5. TEM micrograph of Al-8.4Fe-3.6Ce deformed 25% at 773 K at a strain rate of 1×10^{-5} sec^{-1}. Arrows indicate twinned particles.

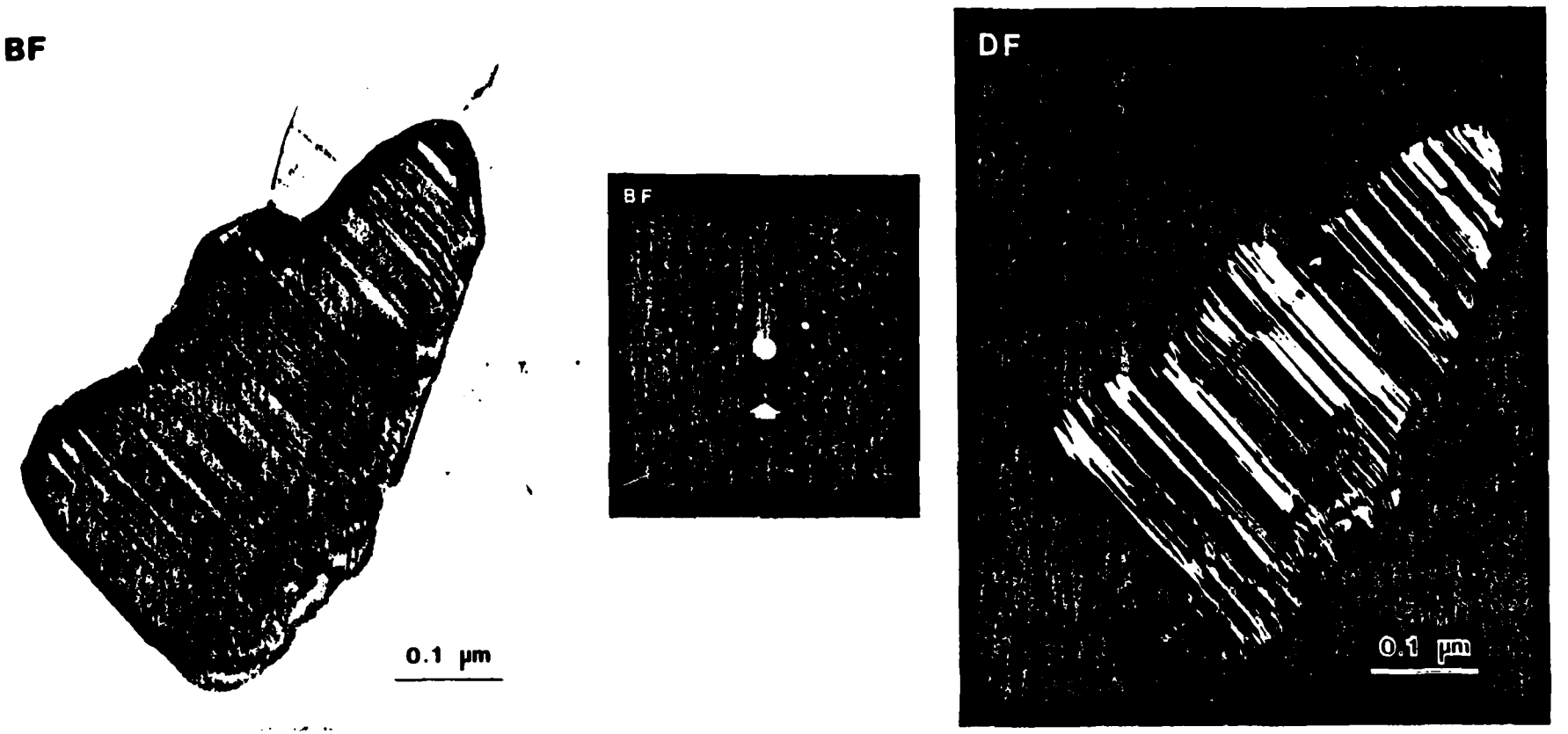

Figure 6. Bright field - dark field pair of TEM micrographs showing a twinned particle in Al-8.4Fe-3.6Ce deformed 25% at 773 K at a strain rate of 1×10^{-5} sec^{-1}. Diffraction spot used to form centered dark field image is indicated (arrow).

TEM micro-diffraction techniques are currently being used to try and identify the twinned particles. Although this part of the investigation is by no means complete, the data collected to date suggest that the twinned particles are probably monoclinic $Al_{13}Fe_4$, which is known to twin (Ref. 2).

IV. Summary

Work performed in the past year has shown that the loss in strength of Al-8.4$^{w}/_{o}$Fe-3.6$^{w}/_{o}$Ce at elevated temperatures is due to the twinning of second phase particles during deformation. In addition, TEM micro-diffraction experiments indicate that these particles are probably monoclinic, $Al_{13}Fe_4$. Microstructural coarsening also contributes to the softening of the AlFeCe alloy at elevated temperatures. However, the amount of softening attributable to microstructural coarsening has been shown to be only a small fraction of the softening actually observed.

REFERENCES

1. W.C. Oliver and W.D. Nix, Acta Met., vol. 30, 1335 (1982).

2. P.J. Black, Acta Cryst., vol. 8, 43 (1955).

C.

CHARACTERIZATION STUDIES OF MECHANICALLY ALLOYED Al-8.4% Fe - 3.4% Ce POWDERS

Mechanical alloying has been used to modify the structure of Al - 8.4% Fe - 3.4% Ce powders made by RSR techniques. The purpose of this work is to investigate the possible beneficial effects of mechanical alloying on the structure and properties of this alloy. The alloy is of interest because of its potential for high temperature structural applications. Additions of iron and cerium to aluminum by RSR techniques have led to the development of alloys with excellent strengths at elevated temperatures [1,2]. However, even these alloys lose their strengths at very high temperatures and other developments are needed to achieve useful strengths in the temperature range 350 - 400°C.

Mechanical alloying is expected to influence the structure of Al-Fe-Ce in several different ways. The repeated fracturing and cold welding that occurs in mechanical alloying is expected to refine the structure by redistributing the existing phases and perhaps, causing new, more stable phases to form. In addition, the presence of carbon and oxygen in the milling environment is expected to lead to the formation of stable dispersoids such as Al_2O_3 and Al_4C_3 [3]. These more stable phases are likely to produce dramatic improvements in strength at temperatures above 400°C.

I. Experimental Procedure

Batches of Al-Fe-Ce powders (4.9 g) with 0.1 g of a processing control agent, Nopcowax - 22 (2% of the batch) mixed under a nitrogen atmosphere have been ball milled with 31 steel balls in a sealed steel can at various

processing times. A high energy ball mill, Spex No. 8000 was used in each case. In order to follow mechanical alloying and observe the final stage of processing, separate characterization analyses of each batch have been made. These characterization studies are (i) Size analysis-Coulter Counter and Sieve measurements (ii) Shape analysis-SEM studies (iii) Hardness measurements (iv) Thermal analysis-Differential Scanning Calorimetry (DSC), and (v) Mass Spectroscopy analysis.

2. Results

The as-received powders have a nominal particle size range of 25-50 μm and their shapes are nodular-spheroidal. As the processing goes on, the particles first become flaky and then equiaxed. The size distribution also changes during processing. Steady state processing, on the completion of mechanical alloying, is reached when the processed powders have developed equiaxed shapes and their size distribution is uniform. This state is assumed to have been reached after 120 minutes of processing. Figure 1 shows a Coulter Counter plot of the size distribution of the alloy processed for 120 minutes. The size distribution is achieved with relatively small deviations and statistical discrepancies between different test trials. Processing times beyond 120 minutes indicated that steady state had been achieved. The variation in hardness shown in Figure 2 indicates a saturation hardness and hence, steady state after 120 minutes. Therefore, 120 minutes of processing has been chosen as the optimum processing time for further thermomechanical treatments.

Since the melting point of aluminum is low and its ductility high, small amounts of organic wax lubricant have been added to the powders to allow

work hardening and fracture and to delay cold welding. The lubricant or surfactant introduces about 1.5% carbon into each batch and it decomposes into the alloy at certain intermediate processing times. It is possible to follow this decomposition with DSC measurements. As shown in Figure 3, a spike is found in the DSC spectrum at 140°C. This is due to melting of the lubricant. After mechanically alloying for 25 minutes (Figure 4) this spike is no longer present. This indicates that the lubricant is no longer present and that the consituents of the lubricant have been worked into the powders. Although the surfactant completely decomposes, the purpose of simultaneous fracturing and welding in mechanical alloying is not lost and the dynamics of processing prevail until it reaches a steady state.

Aluminum powders should contain the least amount of water or hydration to prevent H_2 evolution and porosity cracking during consolidation. A mass spectroscopy analysis has been done on the fully processed powders. From the liberation characteristics of organic species, a degassing temperature of 430 C has been selected for further thermomechanical treatments.

REFERENCES

1. S.L. Langenbeck et.al., Elevated Temperature Aluminum Alloy Development, 1st Interim Report,Contract No.F33615-81-C-5096, October 1981.

2. L.F. Mondolfo, Aluminum Alloys: Structure and Properties, Butterworth and Co., Ltd., London, 1976, pp.468.

3. P.S. Gilman, The Development of Aluminum-Aluminum Oxide Alloys by Mechanical Alloying, Ph.D. Thesis, Stanford University, March 1979.

Figure 1.Coulter Counter size distribution of Al-8.4%Fe-3.4%Ce powders mechanically alloyed for 120 minutes.

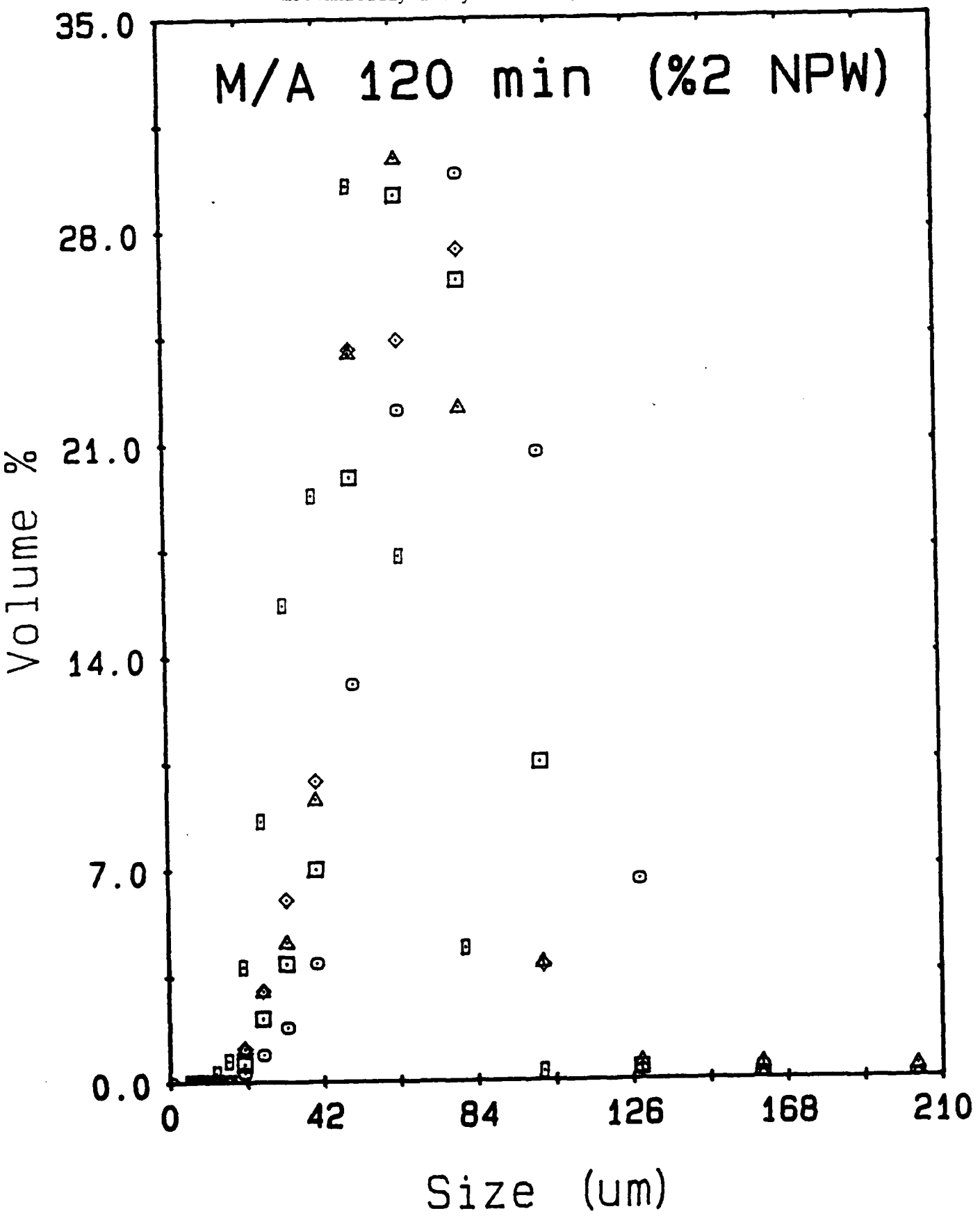

Figure 2. Hardness of Al-8.4%Fe-3.4%Ce owders as a function of alloying .

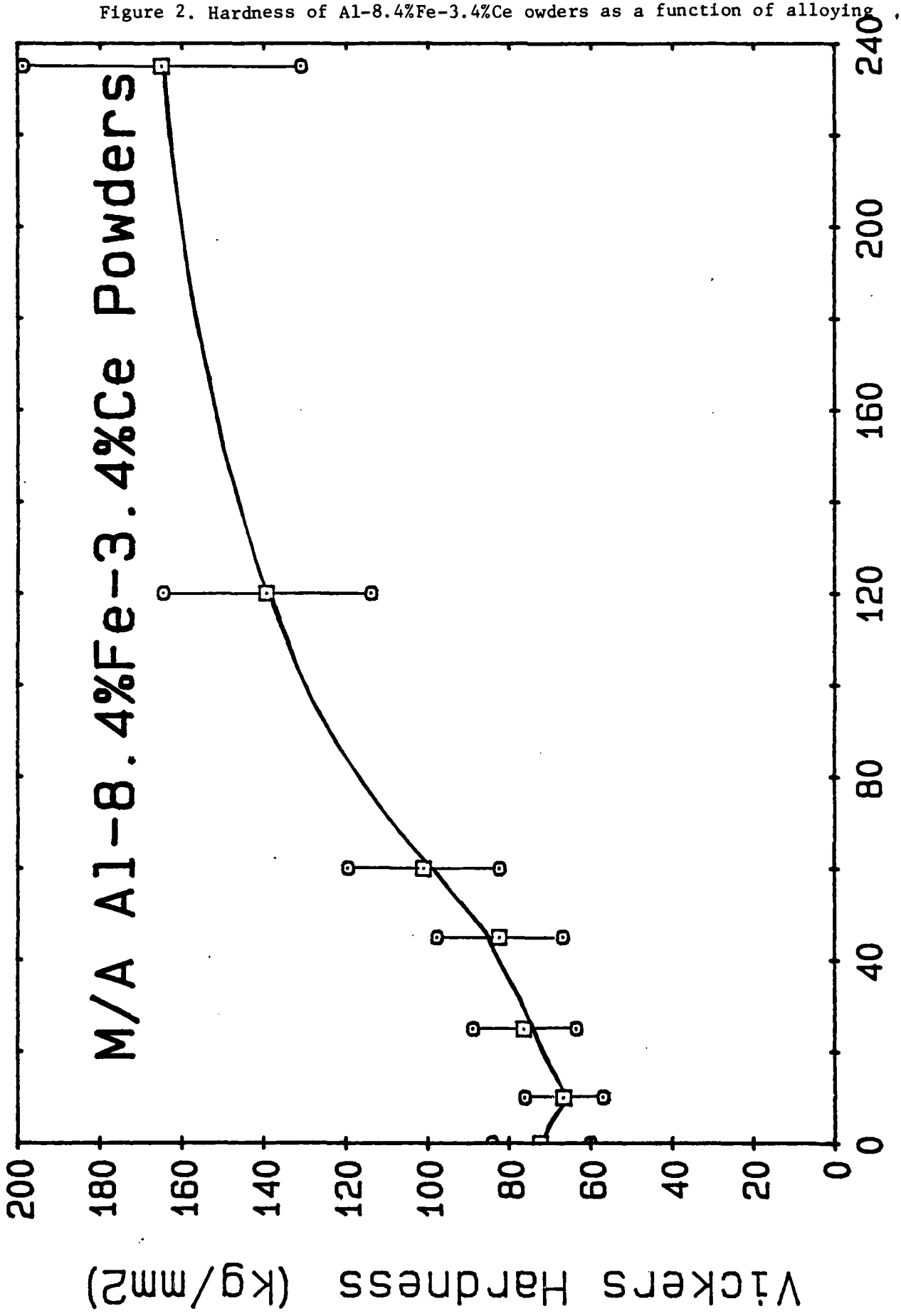

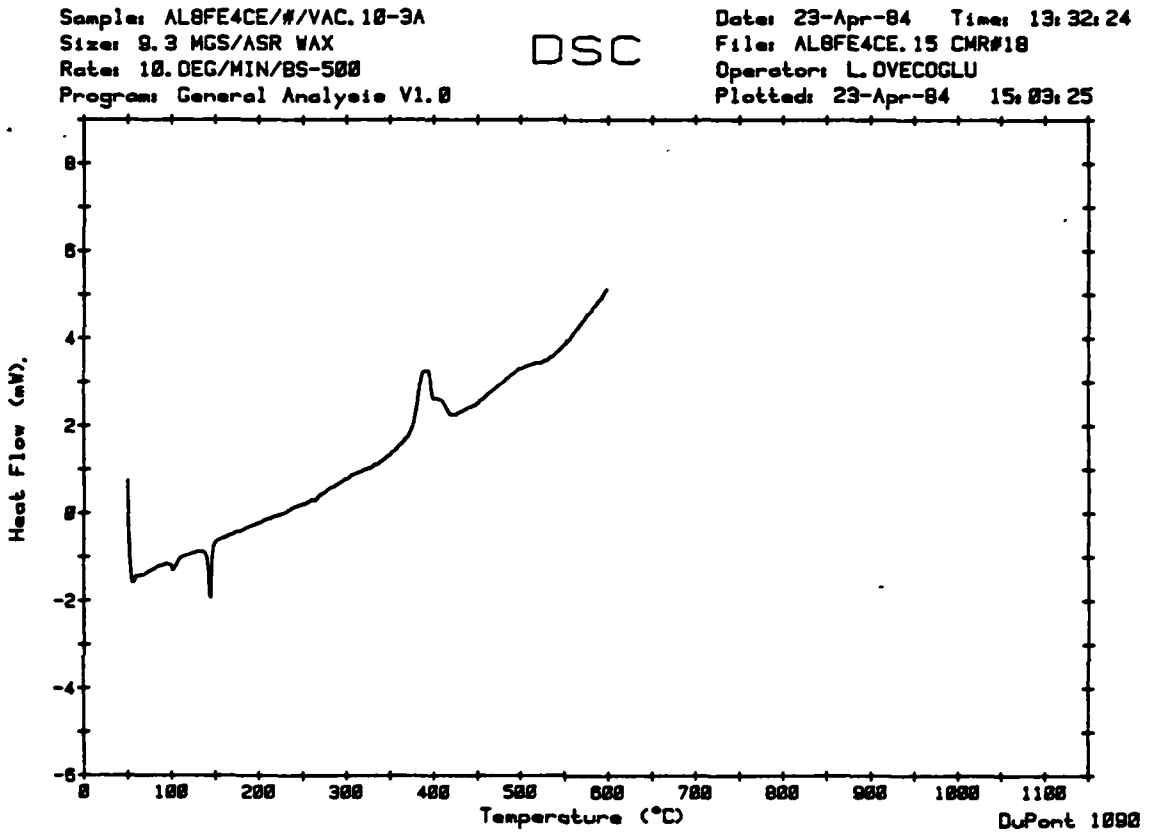

Figure 3.DSC data of Al-8.4%Fe-3.4%Ce as-received powders.

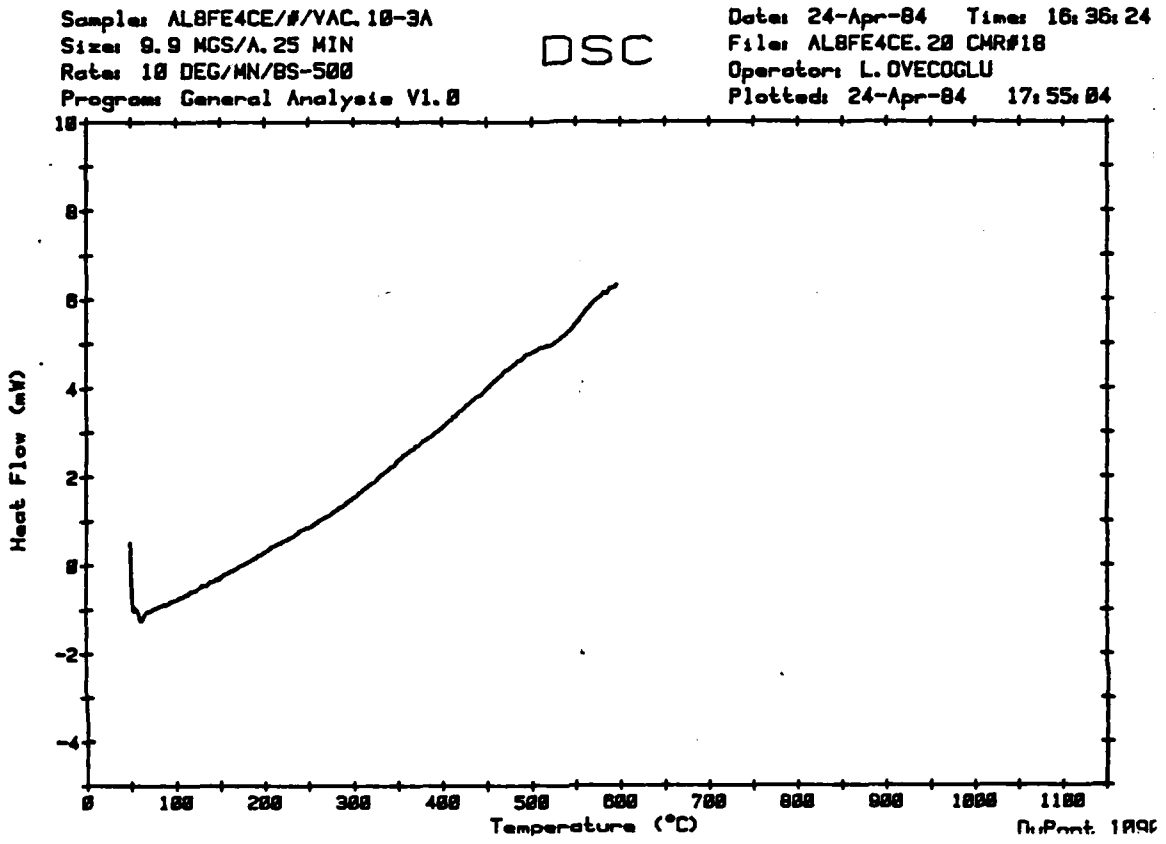

Figure 4. DSC data of Al-8.4%Fe-3.4%Ce powders mechanically alloyed for 25 minutes.

D.

DEVELOPMENT OF TECHNIQUES FOR PREPARING THIN FOILS FROM POWDERS FOR TEM STUDIES

The characterization of metallic powders, such as those produced by rapid solidification, is presently a difficult task. The transmission electron microscope (TEM) is a powerful characterization tool, but TEM sample preparation for the as-powder state has long been a problem. A successful TEM sample preparation method for powders is required.

We have developed a method of TEM powder sample preparation that has showed encouraging initial results. Presently, we are working to optimize the present method by using more sophisticated sample preparation equipment. Considerable improvements in sample quality are expected.

The sample preparation method that we have developed involves mixing the powders with an adhesive to produce a bulk composite solid. The choice of adhesive is crucial in order to get high adhesion and comparable ion milling rates between the powder phase and the adhesive phase. The bulk composite is sectioned, but into 3 mm diameter discs, and mechanically ground to a thickness of typically 120 μm. An ion milling machine performs the final thinning.

The method described above has been used to make several samples from Al-Fe-Ce powders in the as-received state and in the mechanically alloyed state. Bright field micrographs, diffraction patterns, and energy dispersive spectroscopy spectra taken from these specimens demonstrate the feasibility of this technique. The results are encouraging, and improved TEM results are expected to come from current work to optimize the sample preparation technique.

Considerable improvements in sample quality are expected from using a "Dimpler" machine to produce a polished concave depression in the center of the 3 mm specimen disk. Since the center thickness of such a disk is very thin (20 μm) less ion milling is required; and hence the surface irregularities associated with extended ion milling are minimized.

As the sample preparation method is perfected, characterization of Al-Fe-Ce alloy powders at various stages of mechanical processing is being performed.

III. PUBLICATIONS, REPORTS AND DISSERTATIONS RELATING TO THIS AND PREVIOUS AFOSR GRANTS ON OXIDE DISPERSION STRENGTHENED METALS

A. Publications

1. J. H. Holbrook and W. D. Nix, "Edge Dislocation Climb over Non-Deformable Circular Inclusions", Metall. Trans., 5, 1033 (1974).

2. M. Vikram Rao and W. D. Nix, "Creep in Binary Solid Solutions: A Possible Explanation for Anomalous Behavior", Scripta Met., 7, 1255 (1973).

3. M. A. Burke and W. D. Nix, "Plastic Instabilities in Tension Creep", Acta Met., 23, 793 (1975).

4. R. W. Lund and W. D. Nix, "On High Creep Activation Energies for Dispersion Strengthened Metals", Metall. Trans., 6A, 1329 (1975).

5. R. W. Lund and W. D. Nix, "High Temperature Creep of Ni-20Cr-2ThO_2 Single Crystals", Acta Met., 24, 469 (1976).

6. G. M. Pharr and W. D. Nix, "A Comparison of the Orowan Stress with the Threshold Stress for Creep for Ni-20Cr-2ThO_2 Single Crystals", Scripta Met., 10, 1007 (1976).

7. J. H. Hausselt and W. D. Nix, "Dislocation Structure of Ni-20Cr-2ThO_2 After High Temperature Deformation", Acta Met., 25, 595 (1977).

8. J. H. Hausselt and W. D. Nix, "A Model for High Temperature Deformation of Dispersion Strengthened Metals Based on Substructural Observations in Ni-20Cr-2ThO_2", Acta Met., 25, 1491 (1977).

9. R. F. Singer, W. Blum and W. D. Nix, "The Influence of Second Phase Particles on the Free Dislocation Density During Creep of Stainless Steel", Scripta Met., 14, 755 (1980).

10. R. F. Singer, W. C. Oliver and W. D. Nix, "Identification of Dispersoid Phases Created in Aluminum During Mechanical Alloying", Metall. Trans., 11A, 1895 (1980).

11. P. S. Gilman and W. D. Nix, "The Structure and Properties of Al-Al_2O_3 Alloys Produced by Mechanical Alloying:Powder Processing and Resultant Powder Structures",Metall. Trans. 12A, 813 (1981).

12. W. C. Oliver and W. D. Nix, "The Effects of Strain Hardening in the Hydrostatic Extrusion of Axisymmetric Bi-Metal Rods", Metals Technology, February, 75 (1981).

13. W. D. Nix, "The Effects of Grain Shape on Nabarro-Herring and Coble Creep Processes", Metals Forum, 4, 38 (1981).

14. W. C. Oliver and W. D. Nix, "High Temperature Deformation of Oxide Dispersion Strengthened Al and Al-Mg Solid Solutions", Acta Metall., 30, 1335 (1982).

15. D. M. Barnett, W. C. Oliver and W. D. Nix, "The Binding Force Between and Edge Dislocation and a Fermi-Dirac Solute Atmosphere", Acta Metall., 30, 673 (1982).

16. D. M. Barnett, G. Wong and W. D. Nix, "The Binding Force Between a Peierls-Nabarro Edge Dislocation and a Fermi-Dirac Solute Atmosphere", Acta Metall., 30, 2053 (1982).

17. J. K. Gregory, J. C. Gibeling and W. D. Nix, "High Temperature Deformation of Ultra-Fine-Grained Oxide Dispersion Strengthened Alloys" (to be published in Metall. Trans.).

18. D. J. Srolovitz, M. J. Luton, R. Petkovic-Luton, D. M. Barnett and W. D. Nix, "Diffusionally Modified Dislocation-Particle Elastic Interactions" , Acta Metall., 32, 1079 (1984).

19. J. K. Gregory, J. C. Gibeling and W. D. Nix, "High Temperature Deformation of Extremely Fine Grained MA 754 and MA 6000", Fourth RISØ International Symposium on Metallurgy and Materials Science, Roskilde, Denmark, September, 1983.

20. W. D. Nix, "On Some Fundamental Aspects of Superplastic Flow" (to be published in Proceedings of Superplastic Forming Symposium, 1984).

21. J. J. Stephens and W. D. Nix, "Creep and Fracture of Inconel MA 754 At Elevated Temperatures", in Superalloys 1984, Edited by M. Gell et al. Proceedings of the Fifth International Symposium on Superalloys, AIME, 1984, p.329.

22. J. S. Wang, J. J. Stephens and W. D. Nix, "A Statistical Analysis of Cavity Nucleation at Particles in Grain Boundaries" (to be published in Acta Metall.).

23. J. J. Stephens and S. Spooner, "Determination of Dispersoid Size Distributions in Inconel MA 754 by Small Angle X-ray Scattering" (submitted, 1984)

24. J. J. Stephens and W. D. Nix, "The Effect of Grain Morphology on Longitudinal Creep Properties of Inconel MA 754 at Elevated Temperatures" (Submitted to Metall. Trans. 1984).

25. J. J. Stephens and W. D. Nix, "Constrained Cavity Growth Models of Longitudinal Creep Deformation of Oxide Dispersion Strengthened Alloys" (Submitted to Metall. Trans.).

B. Ph.D. Dissertations

1. R. W. Lund, "A Study of High Temperature Creep of Dispersion Strengthened Ni and Ni-20Cr", Ph.D. Dissertation, Stanford University (1975).

2. J. H. Holbrook, "A Theoretical Investigation of Creep of Dispersion Strengthened Crystals", Ph.D. Dissertation, Stanford University (1976).

3. P. S. Gilman, "The Development of Aluminum-Aluminum Oxide Alloys by Mechanical Alloying", Ph.D. Dissertation, Stanford University (1979).

4. W. C. Oliver, "Strengthening Phases and Deformation Mechanisms in Dispersion Strengthened Solid Solutions and Pure Metals", Ph.D. Dissertation, Stanford University (1981).

5. J. K. Gregory, "Superplastic Deformation in Oxide Dispersion Strengthened Nickel Base Superalloys", Ph.D. Dissertation, Stanford University (1983).

6. J. J. Stephens, "Creep and Fracture of an Ittria Dispersed Nickel-Chromium Alloy", Ph.D. Dissertation, Stanford University (1984).

C. Oral Presentations (Speaker Underlined)

1. W. D. Nix, "On the Existence of Steady State Creep", Department of Mechanical Engineering, University of Colorado, Boulder, Colorado (December, 1973).

2. W. D. Nix, "Plastic Instabilities in Tension Creep", Air Force Conference on: Fracture and Fatigue of Two Phase Materials - Effects of Plastic Instability, Fairborn, Ohio (September, 1974).

3. W. D. Nix, "High Temperature Creep of Dispersion Hardened Single Crystals", TMS-AIME (invited paper), University of Toronto (May, 1975).

4. W. D. Nix, "When are Back (Threshold) Stresses Meaningful ?" 1977 Gordon Conference on Physical Metallurgy, Holderness School, Plymouth, N. H., June, 1977. (Invited paper).

5. P. S. Gilman and W. D. Nix, "Mechanical Alloying of Al-Al_2O_3 Alloys", presented at 1978 Spring meeting of AIME in Denver.

6. W. C. Oliver, R. F. Singer and W. D. Nix, "Formation and Identification of Particles in Dispersion Strengthened Aluminum", presented at 1980 Spring Meeting of AIME in Las Vegas.

7. W. C. Oliver, "Mechanical Alloying", presented at Department of Materials Science and Engineering, Industrial Affiliates Meeting at Stanford, June, 1980.

8. W. D. Nix, "Creep of Dispersion Strengthened Metals", presented at EXXON Research Laboratory, Linden, N.J., February, 1980.

9. J. K. Gregory, R. Sinclair and W. D. Nix, "Abnormal Grains in MA753", Annual Meeting of AIME, Chicago, February, 1981.

10. J. K. Gregory, J. C. Gibeling and W. D. Nix, "Superplastic Behavior in MA 6000E", International Symposium on Superplastic Forming of Structured Alloys, San Diego, California, June, 1982.

11. J. K. Gregory and W. D. Nix, "A Model for Superplastic Flow Based on the Coupling of Power Law Creep and Diffusional Deformation", International Symposium on Superplastic Forming of Structural Alloys, San Diego, California, June, 1982 (Poster Session).

12. J. K. Gregory and W. D. Nix, "Flow in an Ultra-Fine Grained Nickel Base Alloy", Poster Session, 1983, Gordon Conference on Physical Metallergy, Holderness School, Plymouth, N.H., June, 1983.

13. J. K. Gregory, J. C. Gibeling and W. D. Nix, "High Temperature Deformation of Extremely Fine Grained MA 754 and MA 6000", Fourth RISØ International Symposium on Metallurgy and Materials Science, Roskilde, Denmark, September, 1983.

14. J. J. Stephens, J. C. Gibeling and W. D. Nix, "Creep and Fracture of MA 754 at Elevated Temperatures", Special Symposium: Physical Metallurgy of High Temperature Alloys, TMS-AIME Fall Meeting, Philadelphia, PA, October, 1983.

15. W. D. Nix, "On Some Fundamental Aspects of Superplastic Flow", Superplastic Forming Symposium, WESTEC 84, Los Angeles, March 1984.

16. J. J. Stephens, J. B. Kortright and S. Spooner, "Particle Size Distributions in Oxide Dispersion Strengthened Alloys", presented at 1984 Spring Meeting of AIME in Los Angeles.

17. J. J. Stephens and W. D. Nix, "Creep and Fracture of Inconel MA 754 at Elevated Temperatures", Fifth International Symposium on Superalloys, Seven Springs Mountain Resort, 7-11 October 1984.

IV. PROFESSIONAL PERSONNEL

The following personnel of the Department of Materials Science and Engineering at Stanford have been engaged in this research program:

Principal Investigator:

Dr. William D. Nix, Professor

Senior Research Associate:

Dr. Jeffery C. Gibeling

Graduate Research Assistants:

Mr. John J. Stephens	B.S.	Cornell University
	M.S.	Stevens Institute of Technology
Mr. M. Lufti Ovecoglu	B.S.	Middle East Technical University, Ankara
	M.S.	Middle East Technical University, Ankara
Mr. Robert Hsieh	B.S.	Northwestern University
Ms Deborah L. Yaney	B.A.	William and Mary
	M.S.	Colorado School of Mines

END

FILMED

4-85

DTIC